Ryerson University
Digital Commons @ Ryerson

Theses and dissertations

1-1-2012

Non-Invasive Measurement Of Tissue Chromophore Concentrations And Cerebral Blood Flow Using Broad-Band Continuous Wave Near Infrared Spectroscopy

Hadi Zabihi-Yeganeh
Ryerson University

Follow this and additional works at: http://digitalcommons.ryerson.ca/dissertations

Part of the Medical Biophysics Commons

Recommended Citation
Zabihi-Yeganeh, Hadi, "Non-Invasive Measurement Of Tissue Chromophore Concentrations And Cerebral Blood Flow Using Broad-Band Continuous Wave Near Infrared Spectroscopy" (2012). *Theses and dissertations.* Paper 1693.

This Thesis is brought to you for free and open access by Digital Commons @ Ryerson. It has been accepted for inclusion in Theses and dissertations by an authorized administrator of Digital Commons @ Ryerson. For more information, please contact bcameron@ryerson.ca.

NON-INVASIVE MEASUREMENT OF TISSUE CHROMOPHORE CONCENTRATIONS AND CEREBRAL BLOOD FLOW USING BROAD-BAND CONTINUOUS WAVE NEAR INFRARED SPECTROSCOPY

by

Hadi Zabihi-Yeganeh

B.Sc., Applied Physics, University of Tehran, Iran, 1997

A thesis

presented to Ryerson University

in partial fulfillment of the

requirements for the degree of

Master of Science

in the Program of

Biomedical Physics

Toronto, Ontario, Canada, 2012

© Hadi Zabihi-Yeganeh 2012

Author's Declaration

AUTHOR'S DECLARATION FOR ELECTRONIC SUBMISSION OF A THESIS

I hereby declare that I am the sole author of this thesis. This is a true copy of the thesis, including any required final revisions, as accepted by my examiners.

I authorize Ryerson University to lend this thesis to other institutions or individuals for the purpose of scholarly research.

I further authorize Ryerson University to reproduce this thesis by photocopying or by other means, in total or in part, at the request of other institutions or individuals for the purpose of scholarly research.

I understand that my thesis may be made electronically available to the public.

Hadi Zabihi-Yeganeh

Non-invasive Measurement of tissue chromophore concentrations and Cerebral Blood Flow Using Broadband Continuous Wave Near-infrared Spectroscopy

Hadi Zabihi-Yeganeh

M.Sc., Bio-medical Physics, Ryerson University, 2012

Abstract

We present a broad-band, continuous wave spectral approach to quantify the baseline optical properties of tissue, in particular the absolute absorption and scattering properties and changes in the concentrations of chromophores, which can assist to quantify the regional blood flow from dynamic contrast-enhanced near-infrared spectroscopy data. Experiments were conducted on phantoms and piglets. The baseline optical properties of tissue were determined by performing a multi-parameter wavelength-dependent differential data fit of the near infrared reflectance spectrum between 680 nm and 970 nm of a photon diffusion equation solution for a semi-infinite homogeneous medium. These baseline optical properties of the piglet head tissue were used to quantify the temporal dynamics of the concentration of the intravenously administered contrast agent Indocyanine Green in the piglet brain. The temporal traces of the Indocyanine Green concentration measured by our method were used to estimate the cerebral blood flow using a bolus tracking technique.

Acknowledgements

I would like to acknowledge the people who made this experience possible and memorable, especially my supervisor, Dr. Toronov, who taught and coached me a lot with his wise advices during the program, and for that I am very thankful. I would like to thank my supervisory committee for taking time and giving me their suggestions and constructive inputs during the long meetings that prepared me for successfully completing the program.

I would also like to express my appreciation to my family and friends for their encouragement and support, especially my wife for her patience and understanding, who always put up with my frustration.

I wish to thank my parents, who never stopped encouraging and praying for me from thousands of miles away, which enabled me to move forward and study during the long winter nights.

This work was supported in part by a grant from the Heart and Stroke Foundation of Canada, a discovery grant from the Natural Science and Engineering Research Council, as well as Ryerson University Research Fund, for which I am very grateful.

Table of Contents

List of Tables

List of Figures

List of Abbreviations

NIRS……Near Infrared Spectroscopy

CT……Computed Tomography

RTE……Radiative Transfer Equation

CW……Continuous Wave

FD……Frequency Domain

TD……Time Domain

CCD……Charge-Coupled Device

TCSPC……Time-Correlated Single Photon Counting

PMT……Photo Multiplier Tube

APD……Avalanche Photo Detector

TPSF……Temporal Point Spread Function

ICG……Indocyanine Green

DP……Differential Path length

DPF……Differential Path length Factor

CBF……Cerebral Blood Flow

CBV……Cerebral Blood Volume

MTT……Mean Transit Time

MBLL……Modified Beer Lambert Law

Chapter 1

Introduction

1.1- Light Propagation in Tissue

When light as electromagnetic wave enters biological tissue, wave packets (photons) may be reduced in their energy or redirected. These events are due to absorption or scattering [1]. Absorption causes attenuation of photonic energy while interacting with absorbers in tissue such as various chromophores. The energy can be converted into heat, chemical energy or into photons with smaller energy (in the case of fluorescence or phosphorescence) [1]. Scattering is due to the interaction between photons and regions in tissue such as cells that have different indices of refraction compared to the surrounding environment (refraction), or with particles whose size is close to the wavelength of the incident light (diffraction), still there is different indices of refraction. In the case of elastic scattering no energy is lost but the direction of energy propagation is changed [2]. The scattered photon can have any direction in the 4π solid angle (whole space). However, depending on the wavelength of the incident light and the size and shape of the scattering centre, there are certain rules for the distribution of the preferential direction of the photon which can be expected. The absorption of tissue is represented by the absorption coefficient μ_a, with units $mm^{-1}\ or\ cm^{-1}$, which is defined as the logarithm of light intensity attenuation per unit length [3]. In the case of a scattering event, the scattering coefficient μ_s is defined, with the same units as the absorption ($mm^{-1}\ or\ cm^{-1}$), and represents the reciprocal of the mean free path length between scattering events [3]. In addition to the absorption and scattering coefficients other important optical parameters of the medium are the scattering anisotropy factor, and the refractive index. When the plane wave of light strikes a

small particle, the light energy will be scattered at different angles. The angular distribution of scattered energy depends on the size and shape of the particle as well as the wavelength of the incident light [1, 4]. This introduces a new parameter, called scattering anisotropy factor "g" [5]. This parameter g is the average cosine of scattering angle "Θ". When the light wave strikes a region in the tissue larger than the wavelength of light, with a different refractive index than the surrounding environment, the light will be reflected and refracted at an angle that depends on the relative refractive index "n",which is a function of the wavelength of the incident light. Since tissue is generally composed of at least 70% water (except for fatty tissue), the refractive index for tissue is usually close to 1.3 [1]. The optical properties are different for various tissues. Moreover, they are function of light source, temperature and water content of the tissue as well as tissue composition. Therefore, different tissues interact with the injected light according to their specific optical properties and they require individual consideration in terms of their optical parameters classification [6].

The parameters μ_a and μ_s are the basic optical properties of tissue that characterize the propagation of light in tissue. Instead of μ_s , the reduced scattering coefficient μ'_s which is defined as $(1-g)\mu_s$ can be used to describe the light transport at distances much longer than the mean free path [1].

In order to obtain the optical properties of tissue from macroscopic optical measurements such as light reflectance, a model of light propagation in tissue is required.

The propagation of light in highly scattering media (biological tissue), is best described by transport theory, also called the radiative transfer equation (RTE) [7].

$$[\frac{1}{v}\frac{\partial}{\partial t} + \hat{s} \cdot \nabla + \mu_a(r) + \mu_s(r)]L(r,t,\hat{s}) = \mu_s(r)\int_{4\pi} f(\hat{s},\hat{s}') \cdot L(r,t,\hat{s}')d\hat{s}' + S(r,t,\hat{s}), \quad (1.1)$$

The RTE is a general balance equation which describes the conservation of the energy in the illumination system (can be thought of as a conservation equation for the radiance) and shows the following rule [1, 7]:

Accumulation of light energy within a system $=$ *(flow in* $-$ *flow out) through the system boundaries* $+$ *generation within the system* $-$ *absorption within the system.*

In the Eq. (1.1), $L(r, t, \hat{s})$ is the radiance at position r, traveling in direction $\hat{s}$, at time t, with the units of $Wm^{-2}sr^{-1}(sr = stteradian = unit\ of\ solid\ angle)$. $f(\hat{s}, \hat{s}')$ is the normalized scattering phase function, which represents the probability of a photon scattering into a direction $\hat{s}'$ from direction $\hat{s}$. v is the speed of light in the medium and $\mu_a(r)$, $\mu_s(r)$ are the absorption and scattering coefficients respectively. $S(r, t, \hat{s})$ is the spatial and angular distribution of the light source (source term of photons) at position r, traveling in direction $\hat{s}$, at time t with units of $Wm^{-3}sr^{-1}$.

In practical situations, analytical solutions for the RTE are impossible to obtain and numerical solutions require large amount of computational power and time. Hence, it is necessary to consider approximate approaches. One of these simplified approaches to obtain an analytical solution to the light distribution, is the diffusion equation approximation to the radiative transport equation [8, 9], which is valid in a highly scattering turbid media at distances much larger than the mean free path [10]. In this approximation no particular direction of transport is preferred for a photon being transported. This translates that each time a scattered photon changes its direction, it may be redirected into a new direction with an equal probability. Therefore, all the directions will be distributed isotropically [11]. Since in most biological tissues scattering is dominant over the absorption, $\mu_s(1 - g) \gg \mu_a$ [3] and the source-detector separation distance

are typically much bigger than the mean free path of photons, $SD \gg (\mu'_s + \mu_a)^{-1}$ [12], then diffusion equation can be used to model the light distribution in tissue[13, 14, 15], and it has the following general form[16]:

$$\left[\frac{1}{v}\frac{\partial}{\partial t} - \frac{D}{v}\nabla^2 + \mu_a(r)\right] U(r,t) = \frac{1}{v} q_0(r,t) \tag{1.2}$$

Where, $U(r,t) = \frac{1}{v}\int L(r,t,\hat{s})d\hat{s}$, gives the photon density at position r and time t, in units of "Jcm^{-3}", v is the speed of light in the medium, $D = \frac{v}{(3\mu_a + 3\mu'_s)}$ is the diffusion coefficient in units of cm^2/s, μ_a, μ'_s are the absorption and reduced scattering coefficients of the medium in units of cm^{-1} and $q_0(r,t)$ is the distribution of the isotropic light source in units of Wcm^{-3}.

1.2- Near Infrared Spectroscopy (NIRS) and its Applications

Since the first publication by Jöbsis in 1977 [17], near infrared spectroscopy (NIRS) has been used in a variety of studies to investigate different physiological and optical properties of tissue, such as cerebral hemodynamics and cerebrovascular functionality [18, 19]. NIRS is an optical technique that uses infrared light in the range of 650 nm to 950 nm (also known as the medical or transparency window) to measure the changes of concentration of light-absorbing molecules (called chromophores) in tissue. In biological tissue at least four main endogenous near infrared chromophores exist: oxy-hemoglobin (HbO2), deoxy-hemoglobin (HHb), fat, and water (H2O). Since the absorption of NIR light is relatively low in the medical window, the light is able to penetrate tissue noninvasively, to a greater extent than other low-energy forms of light, in some cases up to 8 cm [20]. Figure 1-1 shows the NIR specific absorption coefficient spectra of these components in units of. $\mu M^{-1}mm^{-1}$.

Water and fat concentrations do not change much over short periods of time, whereas oxy- and deoxy-hemoglobin concentrations change relative to the metabolism and function of the tissue [17]. Hence, the temporal changes in concentrations of oxy- and deoxy-hemoglobin are of particular importance because they are related to the regional blood flow of the tissue.

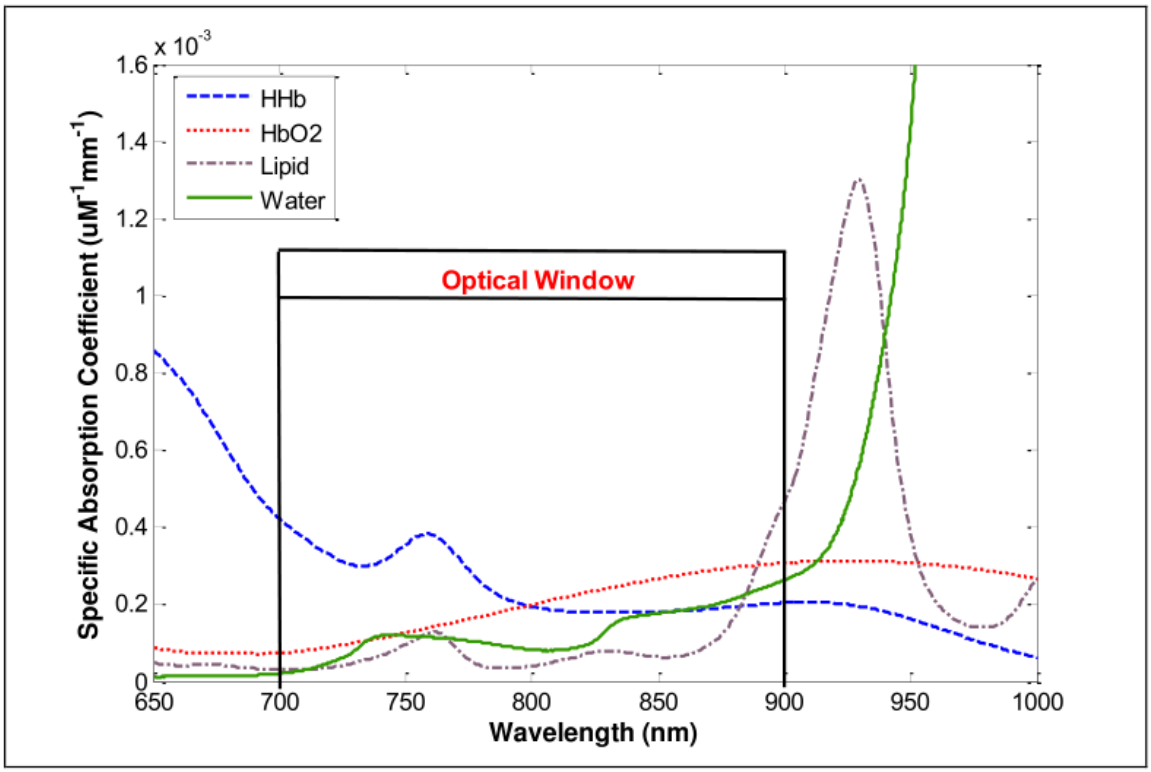

Figure 1-1. The specific absorption coefficient of water, fat (lipid), oxy- and deoxy-hemoglobin as a function of wavelength in the near infrared spectrum

Therefore, by using these changes in the absorption spectra of tissue hemoglobin, useful clinical information about physiological parameters such as blood flow and tissue oxygenation can be obtained.

One of the main advantages of the NIRS technique is non-invasiveness with high biochemical specificity, which is a distinctive feature of the optical spectroscopy. There are many other motivating factors compared to other techniques. Firstly, it provides some information about physiological parameters which are not available to other modalities, such as tissue oxygenation [21]. It also provides high temporal resolution, in the order of "milliseconds" and a lot less restraining factors in comparison with MRI [22]. Moreover, this technique is safe, painless and does not rely on ionizing radiation compared to computed tomography (CT) and positron emission tomography (PET). Although NIRS is a promising diagnostic tool and has been considered and investigated by many scientific groups all around the world, the expected level of NIRS sensitivity, in comparison with other approved modalities, has not been achieved yet. The main reason for this is the extensive light scattering in tissue due to many in-homogeneities at multiple spatial scales. Tissue scattering causes the "diffusion of light", which results in the entangling of the information on the properties of tissue encoded in optical signals. It is hypothesized that such entangling can be decoded to a large extent by using inverse problem methods [23]. Another issue which prevents NIRS instruments being clinically approved at least in the North America is that, signal to noise ratios achievable using existing approaches are not sufficient enough for accurate physiological measurements.

Matcher *et al.* [24] proposed a simple method to measure an important parameter "differential path-length" of photons in a scattering medium using the spectral features of water based on the second differential of absorbance over the wavelength (this will be discussed in details in Section 1.2.4.3), which was a prerequisite to quantify concentration changes of different chromophores by NIRS. The proposed method achieved this without the need for technologically complex time domain (TD) [25] or frequency domain (FD) [26] measurements. It is hypothesized that not only

the second derivative of the absorbance of water spectral features, but also the first differential in the entire NIR spectral band can be utilized to reconstruct the absolute optical properties of tissue without the need to calibrate the probe [27]. This approach was extended to reconstruct both the absorption and the scattering properties of a turbid medium simultaneously from steady-state broadband spectral measurements. Theoretical and experimental evidence were provided that the steady state broadband system had the potential to provide accurate chromophore detection and imaging. In [28] a technique for measuring broadband near infrared absorption spectra of turbid media that used a combination of FD and continuous wave (CW) reflectance methods was presented. Most of the wavelength coverage was provided by a broadband CW measurement, whereas the FD data were acquired at a few selected wavelengths. Absorption and reduced scattering coefficients derived from the FD data were used to calibrate the CW measurements and to estimate scattering at all wavelengths in the spectral window of interest. After these steps, one could determine absorption by comparing the CW reflectance values with the predictions of diffusion theory, wavelength by wavelength.

One of the goals of research on NIRS is to develop standardized imaging platforms that can be utilized as a stand-alone instrument or combined with other modalities such as MRI, CT or ultrasound to provide practical approaches for addressing several key challenges in a variety of clinical diagnostic imaging, such as breast cancer, brain injuries, vasculature diseases, tissue oxygenation, neonatology, as well as small animal imaging.

The focus of this work is on the quantification of the baseline optical properties and changes in the brain tissue chromophore concentration. These are prerequisites to measure cerebral blood flow (CBF) and cerebral blood volume (CBV).

When near infrared light is injected into the tissue, the light scatters in all the directions. However, when a detector is placed at a certain distance from the source to detect scattered light, due to the multiple scattering events, most of the injected photons detected by the detector follow a banana shaped volume to reach the detector (Figure 1-2) [16, 29, 30]. Changes in the amplitude of the backscattered light can be translated to the changes into the concentration of chromophores such as oxy-hemoglobin (HbO2) and deoxy-hemoglobin (HHb) using the modified Beer-Lambert law (MBLL) [29, 31].

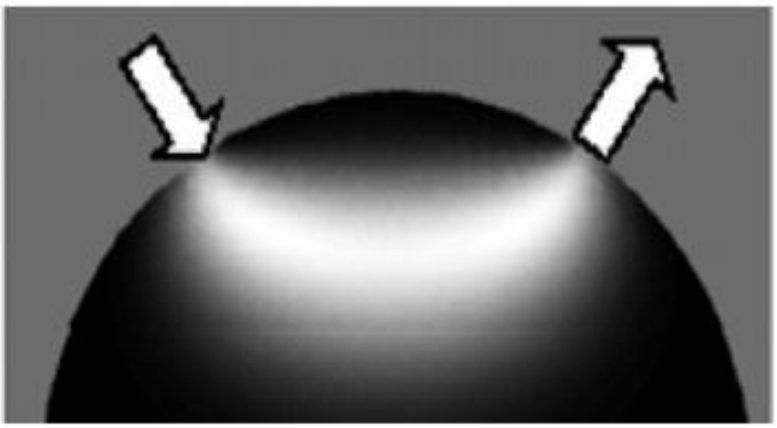

Figure 1-2. Light traveling from source to detector fills a banana-shaped volume

1.2.1- Different NIR Spectroscopy Techniques

Depending on the light delivery protocol, whether it is pulsed or continuous and how frequent the delivery takes place, the method of NIR spectroscopy is defined. There are mainly three types of NIRS: Time-Domain (TD), Frequency-Domain (FD) and Continuous Wave (CW) systems [32, 33]. According to the specific application and considering the advantages and disadvantages, proper technique can be used.

1.2.1.1- Time Domain Systems

In this technique, light is injected to the tissue in the form of an ultra-short pulse (picosecond pulsed laser) resembling a delta function and the intensity of emerging light will be detected as a function of time, using time-correlated single photon counting (TCSPC) detectors [12, 34]. Due to the tissue scattering the pulse is broadened in time. Here a photon counting detector such as a Photo Multiplier Tube (PMT) or an Avalanche Photo Detector (APD) detects and sorts the received photons by their arrival time and their Temporal Point Spread Function (TPSF) shows the distribution of photons arriving time[35]. The shape of this distribution provides important information about optical properties of tissue, such as absorption, scattering and mean optical path length [15, 36] (Figure 1-3).

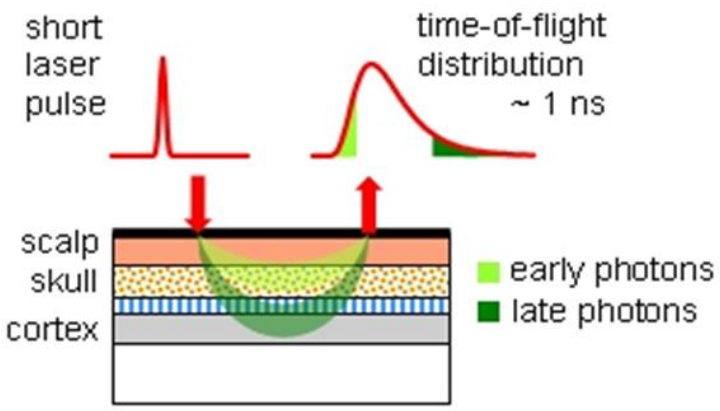

Figure 1-3. An ultra-short laser pulse of light will be broadened in time due to the scattering events

This technique carries good spatial resolution, but has a drawback of slow speed and being expensive.

1.2.1.2 - Frequency Domain Systems

In this type of system, the source of light is a laser diode or Light Emitting Diode (LED), which can be intensity modulated at radio frequency (about 100 MHz or higher). The measurement is usually made of detected light intensity (DC component) as well as phase shift and modulation depth (AC component), in comparison with the input light as shown in Figure 1-4. All this information can give insight into the tissue optical properties such as absorption and scattering coefficients [26, 36]. This system provides similar information as the TD system but at a higher speed and less expensive instrumentation. In fact the time courses of TD and FD systems are related mathematically via the Fourier transform [16]. The main disadvantage of this system is a significant amount of phase noise [36].

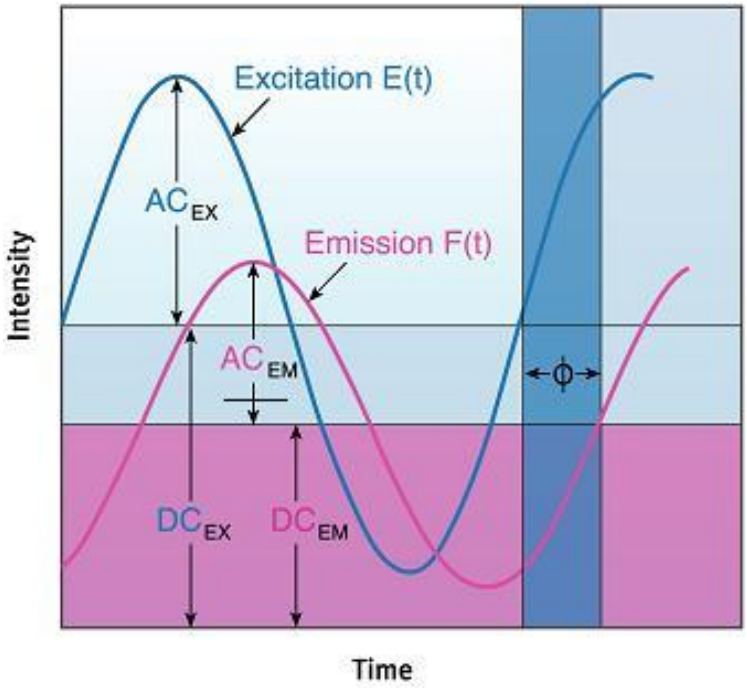

Figure 1-4. Frequency domain instruments employ harmonically modulated sources of light. The measured values are the DC and AC attenuation and the phase shift of the detected signal relative to the source signal.

1.2.1.3 - Continuous Wave Spectroscopy

The continuous wave (CW) systems use either monochromatic or broadband sources of light with constant irradiance. Broadband systems employ detectors such as a cooled charged couple device (CCD) array spectrometer [29]. Figure 1-5 demonstrates the simplified scheme of the system set up, which is used in our Optics Lab. This technique is typically employed to measure changes in absorption ($\Delta\mu_a$) from some arbitrary starting time. The first assumption is that $\Delta\mu_a$is approximately linearly related to the measured attenuation change ΔA, enabling the modified Beer-Lambert law (MBLL) to be used [35]. The second assumption is that the optical path length is constant in time. If it is also assumed that changes in attenuation can only be caused by the changes in concentration of chromophores such as oxy and deoxy-hemoglobin, then these concentrations can be quantified separately from the measurement of ΔA made at different wavelengths [37]:

$$\Delta A = \Delta\mu_a(\lambda) \cdot d \cdot DPF(\lambda) = \left(\varepsilon_\lambda^{HbO2}\Delta[HbO2] + \varepsilon_\lambda^{HHb}\Delta[HHb]\right) \cdot d \cdot DPF(\lambda) \qquad (1.3)$$

where λ is a specific wavelength, d is the source detector distance and $DPF(\lambda)$ is the differential path length factor (will be discussed in Section *1.2.3*). $\Delta[HbO2]$, $\Delta[HHb]$ are the changes in oxy- and deoxy-hemoglobin concentration at the specific wavelength and are dependent on the baseline optical properties. Once the changes in absorption coefficients $\Delta\mu_a^{\lambda 1,2}$ at two different wavelengths λ_1, λ_2 are computed, the changes in the hemoglobin concentrations can be obtained from Eq. (1.3) in the following form [38, 39]:

$$\Delta[HbO2] = \frac{\Delta\mu_a^{\lambda 1}\varepsilon_{HHb}^{\lambda 2} - \Delta\mu_a^{\lambda 2}\varepsilon_{HHb}^{\lambda 1}}{\varepsilon_{HbO2}^{\lambda 1}\varepsilon_{HHb}^{\lambda 2} - \varepsilon_{HHb}^{\lambda 1}\varepsilon_{HbO2}^{\lambda 2}} \qquad (1.4)$$

$$\Delta[HHb] = \frac{\Delta\mu_a^{\lambda 1}\varepsilon_{HbO2}^{\lambda 2} - \Delta\mu_a^{\lambda 2}\varepsilon_{HbO2}^{\lambda 1}}{\varepsilon_{HHb}^{\lambda 1}\varepsilon_{HbO2}^{\lambda 2} - \varepsilon_{HHb}^{\lambda 1}\varepsilon_{HbO2}^{\lambda 2}} \quad (1.5)$$

Where $\varepsilon_{HbO2}^{\lambda 1,2}$ *and* $\varepsilon_{HHb}^{\lambda 1,2}$ are the specific absorption coefficients of oxy- and deoxy-hemoglobin respectively, at wavelengths λ_1 *and* λ_2.

The CW technique has advantages of being relatively inexpensive comparing to TD and FD techniques as well as portability and less complexity, which makes it more suitable for applications in the clinical environments.

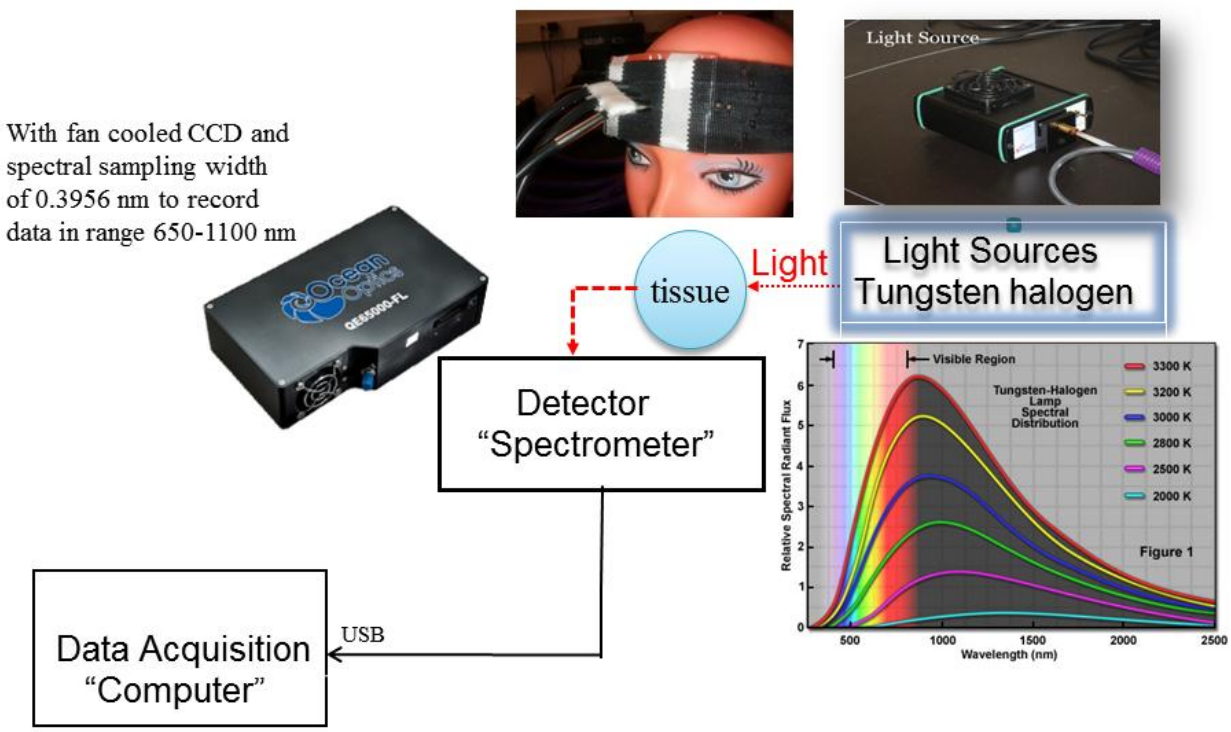

Figure 1-5. Simplified scheme of the NIR continuous wave spectroscopy system set up

1.2.2- Beer-Lambert Law of Absorption

The wavelength dependent absorption coefficient of a chromophore is determined by the product of the extinction coefficient of the chromophore and the concentration of that chromphore [40]. The tissue absorption coefficient is the sum of all the chromophore concentrations weighted by their specific absorption (extinction) coefficients.

$$\mu_a(\lambda) = \varepsilon(\lambda)C \tag{1.6}$$

$$\mu_a^{tissue}(\lambda) = \sum_1^n \varepsilon_n(\lambda)C_n \tag{1.7}$$

where $\mu_a(\lambda)$ is the absorption coefficient in (mm^{-1}), C is the concentration (μM) and $\varepsilon(\lambda)$ is the extinction coefficient in $(mm^{-1}\mu M^{-1})$.

A change in the irradiance of light "dI" due to the absorption is directly proportional to the irradiance of the incident light "I" and the optical path length in the absorbing medium"dl", with the proportionality factor "μ", as follows:

$$dI = -\mu I dl \tag{1.8}$$

where μ is the absorption coefficient. Solving Eq. (1.8) gives the Beer-Lambert Law of absorption [41] as expressed in the following form:

$$I(x) = I_0 e^{-\mu l} \tag{1.9}$$

Using Eq. (1.6), for a light absorbing but non scattering medium we have following equation:

$$A = -log\frac{I}{I_0} = \varepsilon(\lambda)Cl \tag{1.10}$$

This shows the linear relationship between the absorbance of light A, the propagation distance l, and the concentration C of the chromophore.

1.2.3- The Modified Beer-Lambert Law (MBLL)

When the medium scatters light, in addition to the absorption, equation 1.10 must be modified as follows:

$$A = -log\frac{I}{I_0} = \varepsilon(\lambda) \cdot C \cdot DP(\lambda) + G(\lambda) \tag{1.11}$$

to include (1) an additive term G, due to the scattering losses, (2) a multiplier factor, to account for the increased optical path length due to the multiple scattering of the photon in the medium. Hence, the actual mean optical distance (physical distance) of the photon to reach the detector [41] "DP" is the geometrical distance "d" multiplied by the scaling factor known as the differential path length factor, "DPF". Figure 1-6, demonstrates the introduced factor.

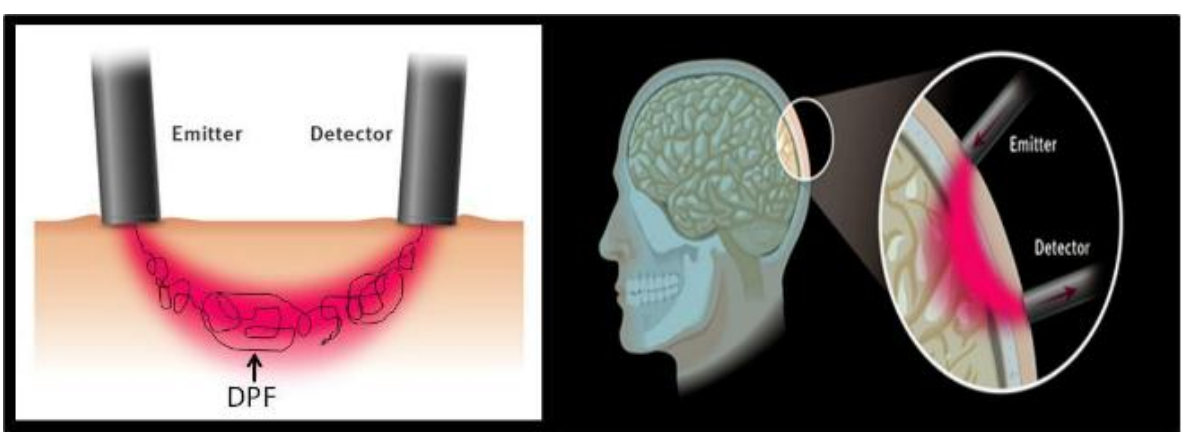

Figure 1-6. Depiction of light distribution from emitter to detector in the tissue and the concept of DPF (adopted from [30])

$$DP = DPF(\lambda) \cdot d \tag{1.12}$$

Considering these two additions, the modified Beer- Lambert law, that applies to an arbitrary geometry and is no longer linear, is expressed as follows [12, 20, and 42]:

$$A = -log\frac{I}{I_0} = \varepsilon(\lambda) \cdot C \cdot d \cdot DPF(\lambda) + G(\lambda) \tag{1.13}$$

Since the value of G is unknown, therefore, equation 1.13 cannot provide the absolute measurement of the chromophore concentration in the target medium from a measure of absolute attenuation. However, assuming G is constant during the measurement period, which is true for a homogeneous medium where the scattering property is constant [43], it is possible to find the chromophore concentration changes from the measured attenuation changes.

$$(A_2 - A_1) = (C_2 - C_1)\varepsilon(\lambda) \cdot d \cdot DPF(\lambda) \tag{1.14}$$

$$\Delta A = \Delta C \cdot \varepsilon(\lambda) \cdot d \cdot DPF(\lambda) \tag{1.15}$$

As the specific absorption coefficient of the chromophore $\varepsilon(\lambda)$ is known and the geometrical distance between the points where the light enters and exits the medium d can be easily measured, the measurement of change in concentration depends on the $DPF(\lambda)$ measurement. There are different techniques that can be used to quantify DPF in tissue as they are described next.

1.2.4- Measurements of Differential Path length Factor (DPF)

1.2.4.1- Time of Flight

A picosecond pulse laser and ultrafast detector can be used to measure the time of flight of the light traveling through the tissue [12] The laser can be tuned in the near infrared range (i.e.

between 740 nm and 920 nm). The system includes precision mirrors to split the laser beam where part of the laser output is taken to the streak camera as a reference time, the other part of the beam is directed to the tissue. The two temporal signals are recorded simultaneously on the same streak image.

The time difference Δt between the light entering the tissue and the mean time of passing light through the tissue is measured from the streak image and used to calculate the DPF in the tissue.

$$DPF = \frac{DP}{d} = \frac{c \cdot \Delta t}{d \cdot n} \tag{1.16}$$

where c is the speed of light in vacuum and n is the index of refraction for tissue (typically taken as 1.33 [44]). The DPF can be calculated from equation 1.16.

1.2.4.2-Frequency-Domain Spectroscopy

A light source is modulated at a specific frequency (usually 100 MHz to 200 MHz) and the phase shift between the AC modulations of light entering and leaving the tissue can be recorded. If this phase shift P is measured in radians, the total distance light travelled through the tissue sample DP can be calculated as follows [45]:

$$DP = \frac{P \cdot c}{2\pi f n} \tag{1.17}$$

where f is the modulation frequency. Note that this technique is capable of measuring the total light path in real time without the need for measuring $d,$ the geometrical distance which might carry inaccuracy of measurement. Specifically, in the case of moving subjects, such as tissue oxygenation measurement in the fetal head during labour or in muscle oxygenation measurement during exercise.

1.2.4.3- Second Derivative Spectroscopy Analysis (SDSA)

This method relies on the broadband spectroscopy (spectral domain rather than time or frequency domain approaches). The differential path length DP can be derived from the broadband absorbance spectrum using the second derivative spectral analysis method, knowing the water concentration of tissue with accuracies of a few percent [46]. This method was first introduced by Matcher *et al* 1994 [24].

It is evident from (1.13) that the attenuation is a function of absorption and reduced scattering coefficients, $A(\mu_a(\lambda), \mu'_s(\lambda))$, and both coefficients are wavelength dependent. Since $DPF\ (\mu_a, \mu'_s)$ and $G(\mu'_s)$ are functions of scattering, so the first and second derivative of the attenuation with respect to the λ is expressed as follows:

$$A' = \frac{dA}{d\lambda} = \frac{d\mu_a}{d\lambda} DPF \cdot d + \frac{dG}{d\lambda} + \mu_a \frac{d(DPF)}{d\lambda} d \qquad (1.18)$$

The 2nd and 3rd terms in equation (1.18) are negligible due to the weak wavelength dependence of the scattering.

$$A'' = \frac{d^2A}{d\lambda^2} = \frac{d^2\mu_a}{d\lambda^2} DPF \cdot d + \frac{d\mu_a}{d\lambda} \frac{d(DPF)}{d\lambda} d \qquad (1.19)$$

For the same reason 2nd term is small compare to the 1st , so we obtain a simplified equation:

$$A'' = \frac{d^2A}{d\lambda^2} = \frac{d^2\mu_a}{d\lambda^2} DP \qquad (1.20)$$

Equation (1.20) shows that the second derivative spectrum of the attenuation is the second derivative of the absorption coefficient scaled by the differential path length. At certain wavelengths (near 820 nm and 970 nm) water absorption spectrum exhibits peaks while other

chromophores have flat spectra without features. Therefore, based on Eq. (1.20), for such spectral bands one can neglect second derivatives of all chromophores other than water. According to Eq. (1.6)

$$\mu_a^{H2O} = C_{H2O} \cdot \varepsilon_{H2O} \tag{1.21}$$

$$\frac{d^2\mu_a^{H2O}}{d\lambda^2} = C_{H2O} \cdot \frac{d^2\varepsilon_{H2O}}{d\lambda^2} \tag{1.22}$$

Then according to Eq. (1.20), one can express the second derivative of the absorption as

$$A'' = \frac{d^2A}{d\lambda^2} = \frac{d^2\varepsilon_{H2O}}{d\lambda^2} \cdot C_{H2O} \cdot DP \tag{1.23}$$

This theory forms the basis of the second derivative spectral analysis method. By performing a least squares fit of the 2nd derivative of attenuation with the corresponding 2nd differential spectrum of water ε''_{H2O} the amplitude of the second derivative spectral feature of water can be determined. The resulting scale factor divided by the known water concentration gives the value of DP.

As it is explained in (Section 1.2), Oxy-hemoglobin, Deoxy-hemoglobin and water are the dominant NIR tissue chromophores. The tissue absorption coefficient μ_a is a sum of absorptions due to all chromophores (see Fig. 1.1). However, at some wavelengths the contributions of some chromophores, in particular water, become sharper and more distinctive in the first and second derivatives spectra as shown in Figure 1-7 (a) and (b).

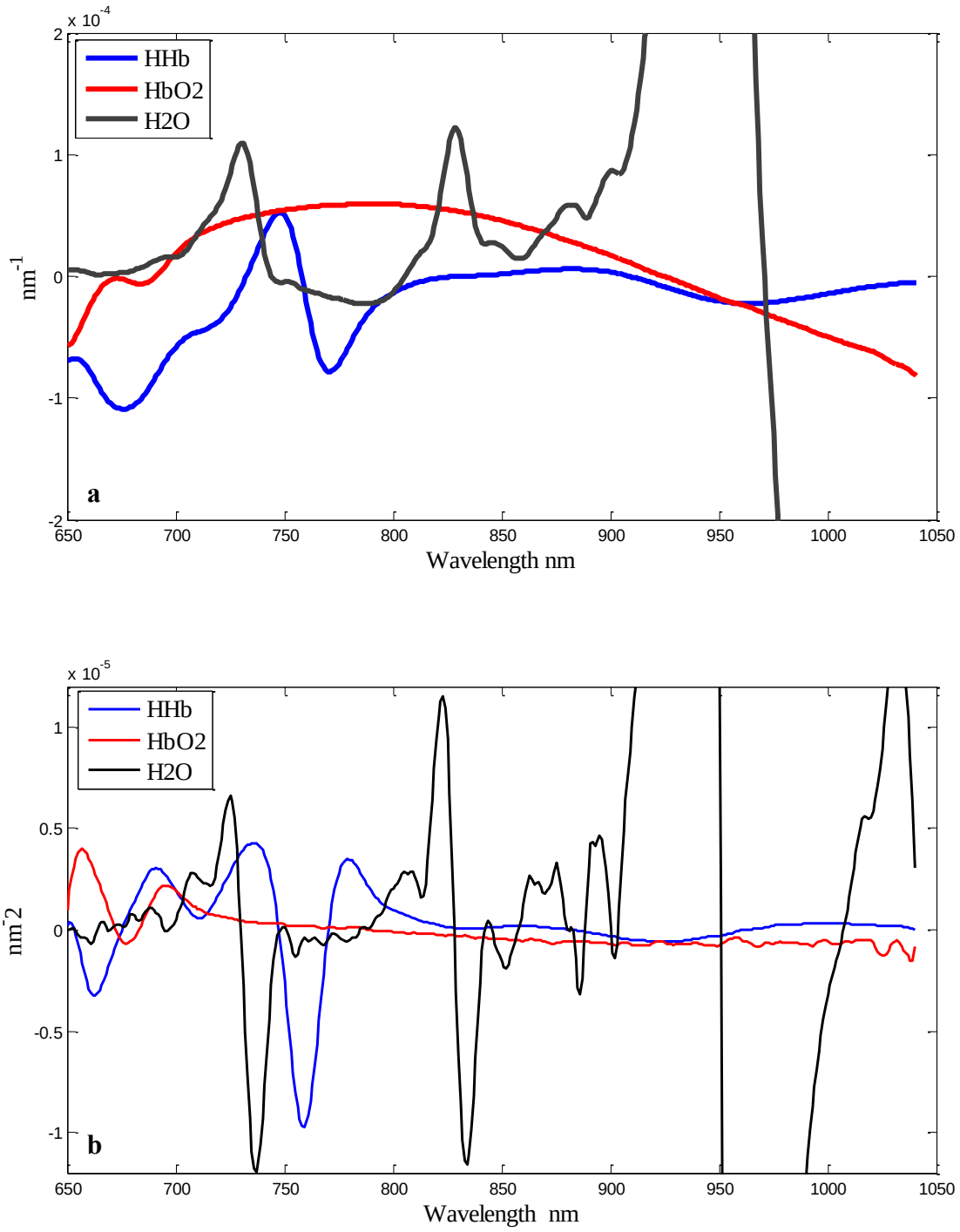

Figure 1-7. (a) First derivative, **(b)** Second derivative spectra of specific absorption coefficients of oxy-hemoglobin, deoxy-hemoglobin and water

1.2.5- Factors Influencing the Differential Path length Factor

Based on experimental studies, it has been shown that differential path length depends on the following factors:

1) Type of the tissue and its composition (tissue inhomogeneity): for example tissues with different water content, such as fat, muscle and bone have different DPFs [24].
2) Wavelength: time domain systems have been used to demonstrate the relationship between the DPF and wavelength (or in other word absorption coefficient), in the neonatal head and adult head, forearm and calf [47]. In all cases with increasing wavelength from 740 nm to 840 nm, the DPF decreased. Hence, it is important to mention the wavelength at which the DPF measurement has been made.
3) Absorption coefficient: The relationship between the DPF and the absorption coefficient can be demonstrated using theoretical data generated using the diffusion equation as a function of absorption coefficient in a medium with different scattering properties, which is shown in Figure 1-8. This figure shows the attenuation of light as a function of μ_a for a medium with the thickness d and various scattering conditions [48]. In general, the DPF value will decrease with increasing absorption coefficient and increase with increasing scattering coefficient.
4) Geometry of the optodes: computer simulation has been used to demonstrate the effect of geometry in DPF measurements [49]. Other than optode spacing, DPF is dependent upon the angle between the tissue surface and the emitter or detector directions.
5) In a highly scattering medium such as tissue the DPF is strongly dependent upon the reduced scattering coefficient

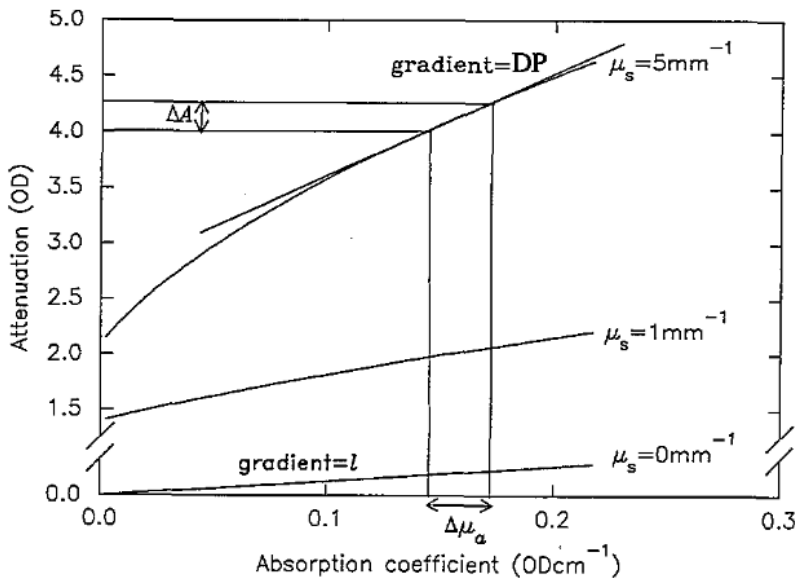

Figure 1-8. Theoretical form of $A(\mu_a)$ obtained using diffusion theory, for different values of scattering coefficient (adopted from [24]).

1.3- Using NIRS to Monitor Cerebral Hemodynamics

The brain is an organ that functions at a high metabolic rate of oxygen most of the time [50] which makes it critically dependent on a highly regulated vascular supply of oxygen and structural substrates. Therefore, monitoring and recording the balance of blood flow and metabolism is very important especially during serious diseases. As one of many applications of the near infrared spectroscopy, cerebral hemodynamics monitoring is of particular importance in order to understand mechanisms involved in the brain function and the development of diagnostic tools in cerebrovascular disorders [51].

A number of near infrared spectroscopy studies have demonstrated that changes in hemodynamics related to the functional brain activity can be obtained in human studies [52, 53, 54 and 21]. Fast changes in optical properties of cerebral tissue can be measured using NIRS [21, 55 and 56]. Within a few milliseconds after stimulation, a neuronal signal due to the change in

the scattering properties of the neurons will occur upon the activation [56]. The hemodynamic response of the brain can be measured in few seconds after the activation, as the increasing oxygen consumption which leads to changes in oxy- and deoxy-hemoglobin concentrations incurring changes in the optical properties of the tissue [54, 21 and 56].

1.3.1- Bolus Tracking Method to Measure CBF

The measurement of CBF using near infrared spectroscopy technique requires the use of Indocyanine Green (ICG) as an inert intravascular tracer [57, 58]. ICG is a strong near infrared light absorbing dye that binds the plasma albumin once is injected into the blood stream and is not expected to cross blood brain barrier. Therefore, it remains in the circulation system for an extended period of time. Figure 1-9. shows the specific absorption spectrum of the ICG.

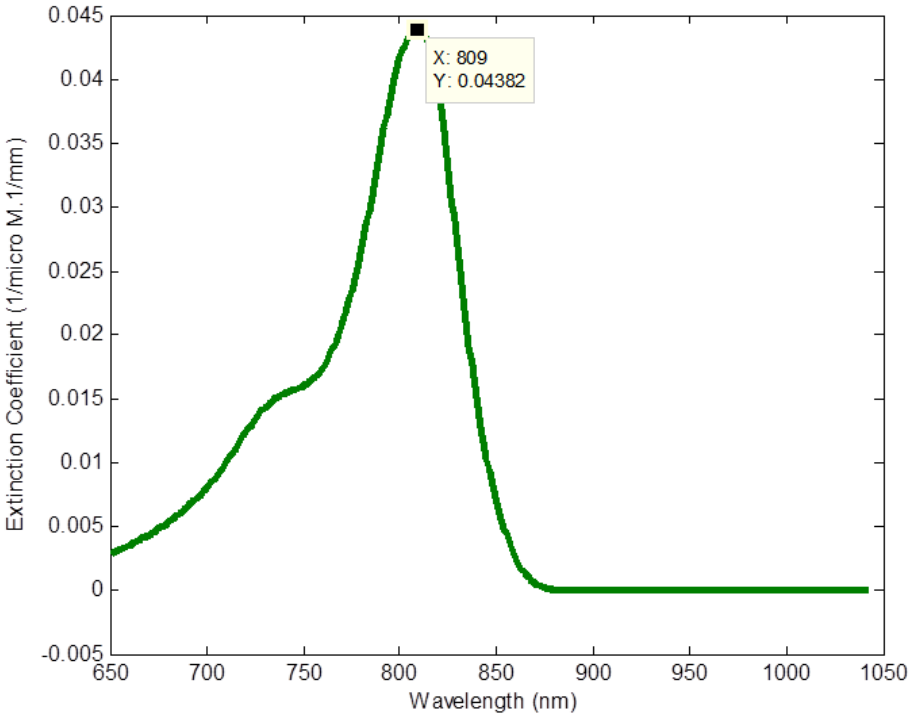

Figure 1-9. Specific absorption spectrum of ICG

CBF can be measured by applying the Fick principle, which states:

$$C_t(t) = CBF \int_0^t (C_a(t) - C_v(t))dt \tag{1.24}$$

where $C_t(t)$, $C_a(t)$ and $C_v(t)$ are the tissue, arterial and venous concentrations of the ICG and CBF is the cerebral blood flow. The Eq. (1.24) shows that CBF is the ratio of the rate of ICG concentration in the brain to the amount of ICG delivered. If it is assumed that there is no venous outflow of the ICG within the minimum cerebrovascular transit time (time interval 0 $to\ t$), then the CBF can be estimated in each time within (0 $to\ t$) by calculating the slope of the tissue concentration curve to the integral of the arterial concentration curve. The arterial ICG concentration $C_a(t)$ can be measured noninvasively by a dye densitometer [59] and the brain ICG concentration by NIRS technique, CBF can thus be estimated.

1.4- Research Objectives

The main goal of this research is to develop a highly sensitive and cost-efficient method of quantifying the optical properties of the brain tissue, non-invasively and consequently the hemodynamic changes in the brain using a broadband (multispectral) continuous wave near infrared spectroscopy technique. This work was initially inspired by the collaboration with the group of scientists (K. St. Lawrence et al.) at Lawson Research Institute, who are interested in the measurements of cerebral blood flow (CBF), using sensitivity of NIR signals to the injected light absorbing dye Indocyanine-Green (ICG). The approach is based on the homogeneous model of the piglet head. The method consists of two steps. First, to obtain the baseline optical properties of the animal's brain by performing a spectral differential fit analysis of the absorbance data in the near infrared range of 650 nm to 950 nm. Second, to find the time course concentration changes of the ICG in the brain. In order to improve the accuracy of these

measurements we used and modified a Matlab software package for the reconstruction of the optical properties of the semi-infinite homogeneous medium from broadband spectral data using the solution to the diffusion equation. As an extra constraint and validation of the results, we applied second differential fit analysis of the absorbance data using the modified Beer-Lambert law to find the DPF and compare with the calculated ones from the first method.

Chapter 2 presents the accepted manuscript to be published in the journal of Biomedical Optics Express on the broadband continuous wave measurements of the baseline and chromophore concentration changes using near infrared spectroscopy technique. Chapter 3 explains a development and modification of the algorithm.used Chapter 4 presents the discussion and conclusions of this work as well as future works.

Chapter 2

Journal Manuscript

BROAD-BAND CONTINUOUS WAVE TECHNIQUE TO MEASURE BASELINE VALUES AND CHANGES IN THE TISSUE CHROMOPHORE CONCENTRATION

Hadi Zabihi Yeganeh[a], Vladislav Toronov[a], Jonathan T. Elliott[b], Mamadou Diop[b], Ting-Yim Lee[b,c] and Keith St. Lawrence[b]

[a]*Ryerson University, Department of Physics,350 Victoria St. Toronto, Ontario M5B 2K3, Canada*

[b]*Lawson Health Research Institute, Imaging Program, London, Ontario N6A 4V2, Canada*

[c]*Imaging Research Laboratories, Robarts Research Institute, London, Ontario N6A 5K8, Canada*

Abstract

We present a broad-band, continuous wave spectral approach to quantify the baseline optical properties of tissue and changes in the concentration of a chromophore, which can assist to quantify the regional blood flow from dynamic contrast-enhanced near-infrared spectroscopy data. Experiments were conducted on phantoms and piglets. The baseline optical properties of tissue were determined by a multi-parameter wavelength-dependent data fit of a photon diffusion equation solution for a homogeneous medium. These baseline optical properties were used to find the changes in Indocyanine green concentration time course in the tissue. The changes were obtained by fitting the dynamic data at the peak wavelength of the chromophore absorption, which were used later to estimate the cerebral blood flow using a bolus tracking method.

2.1- Introduction

Near infrared spectroscopy (NIRS) [56] can be used to measure absolute concentrations and changes of endogenous chromophores such as oxy and de-oxy hemoglobin and exogenous ones such as indocyanine green (ICG) [60]. ICG is a near infrared light absorbing dye which has many clinical applications. To measure absolute optical properties, frequency domain [61] and time domain [62] systems were proposed. In our recent phantom study [63] we have shown that multichannel broadband NIRS can measure optical properties of a two-layer highly scattering medium with the thickness of the top layer close to the adult skull thickness. This method was a generalization of the second-derivative approach proposed earlier by Matcher *et al* in [24]. In the present work we further develop the method of [63] to measure both the baseline optical properties of head tissues and changes in the ICG concentration (*in vivo*). The main methodological challenge of the *in-vivo* tissue measurement compared to the phantom study was a larger number of chromophores. To demonstrate the clinical potential of our method we use the baseline optical properties to measure the time varying concentration of ICG in the animal brain and then use it to measure cerebral blood flow (CBF) by a bolus tracking technique [64, 65]. For validation, the CBF values obtained by NIRS were compared to values obtained with perfusion computed tomography (pCT).

2.2- Materials and Methods

2.2.1- Animal Experiment

The study was approved by the Animal Use Subcommittee of the Canadian Council on Animal Care at the University of Western Ontario. Piglets were tracheotomised and mechanically ventilated while anaesthetized by isoflurane. Cannulas were inserted into each ear for injection of

the NIRS and CT contrast agents. An additional cannula was inserted into a femoral artery to allow blood samples to be collected for gas and glucose analysis. Following the surgical procedure, animals were allowed to stabilize for 1 h before BF measurements were collected. Near-infrared spectroscopy and CT data were collected concomitantly. Cerebral blood flow (CBF) was measured using a bolus-tracking method that requires an intravenous bolus injection of ICG (0.1 mg/kg), followed by continuous measurements of the time-varying concentrations of ICG in arterial blood and brain tissue. Computed tomography (CT) images of CBF were acquired using a LightSpeed QXi multislice CT scanner (GE Healthcare, Milwaukee, Wisconsin) upon injection of 1.0 ml/kg of the iodinated contrast agent iohexol (300 mg I/mL; OmnipaqueTM, GE Healthcare, Waukesha, Wisconsin).

2.2.2- Near-infrared spectroscopy

An in-house-developed continuous-wave broadband spectrometry system was used to collect the near-infrared data [65]. The main components of the system included an illumination unit and a spectrometer consisting of a holographic grating and a cooled charge-coupled device (CCD). The illumination unit was 50Watts quartz, halogen light bulb that was band-pass filtered to remove light outside the 600 to 1000 nm range. The filtered light was coupled to a 2-m fiber optic bundle (emission optode) with a numerical aperture of 0.55 and a 3.5 mm-diam active area. The opposite end of the emission optode was placed on the scalp of the animal and held in position by a specially designed flexible probe holder. Another optical fiber bundle (detection optode) with the same specifications as the emission optode was positioned at 2.7cm distance from the emitter to collect light that traveled through the tissue. Light collected by the detection probe was recorded at intervals of 200 ms.

2.2.3- Algorithm

The light propagation in a turbid medium can be described by radiative transfer theory [66, 67] which in the present application can be reduced to the diffusion approximation [68, 69]. Since the extra-cerebral tissue layer in newborn piglets was very thin (1-2mm), we could approximate the head as a homogeneous medium. There is a solution for semi-infinite homogeneous media which defines the continuous wave photon flux as the following [70]:

$$\psi = \frac{2}{(4\pi)^2}\frac{S}{D}\frac{\exp\left[-\rho\left(\frac{\mu_a}{D}\right)^{\frac{1}{2}}\right]}{\rho^3}\left[1+\rho\left(\frac{\mu_a}{D}\right)^{\frac{1}{2}}\right](z_b+z_0)\left[z+3D\left\{1-\frac{(z_b+z_0)^2+3z^2}{2\rho^2}\right\}\times\left\{\left[3+\frac{\rho^2\frac{\mu_a}{D}}{1+\rho\left(\frac{\mu_a}{D}\right)^{\frac{1}{2}}}\right]\right\}\right], \tag{2.1}$$

where, $D = \frac{1}{3\mu_a+3\mu'_s}$ is the diffusion coefficient and ρ is the source detector distance in the radial coordinate, S is the source strength in photon per second and μ_a and μ'_s are the absorption and reduced scattering coefficients, z_0 and z_b are the boundary approximation parameters and defined by the following expressions [71]:

$$z_0 = 3D \quad , \quad z_b = 2D \tag{2.2}$$

Here it is assumed that all the incident photons are initially scattered at the same depth z_0 and z_b is the negative image source some distance beyond the physical surface so that the fluence rate is set to be zero at that point, this is called extrapolated boundary condition [72].

This model depends on the absorption and reduced scattering coefficients of the medium. The absorption coefficient of the medium can be calculated as:

$$\mu_a = [HbO2]\,\varepsilon(\lambda)_{HbO2} + [HHb]\,\varepsilon(\lambda)_{HHb} + [ICG]\,\varepsilon(\lambda)_{ICG} + (\%FC_{H2O})\mu_{a\,H2O} + (\%FC_{fat})\mu_{a\,fat} \tag{2.3}$$

where, the quantities in square brackets represented the concentration of oxy and deoxy-hemoglobin and *ε(λ)* represented their molar extinction coefficients respectively. $\mu_{a_{H2O}}$ and $\mu_{a_{fat}}$ were the absorption coefficients of water and fat, and (%FC) was their volume fraction.

To model the reduced scattering coefficient spectral dependence, we assumed that μ'_s as a function of wavelength obeys the empirical power law:

$$\mu'_s(\lambda)=M(\lambda/800)^{-\alpha} \tag{2.4}$$

with specific values of "*M*" and "*α*". To obtain the baseline optical properties (without ICG) the procedure was to try all possible combinations of the parameters ([HbO_2], [HHb], (%FC_{H2O}) , *α*, and *M*) to find the best fit of the experimental data curve, using the homogenous diffusion solution Eq.(2.1). Each one of the parameters was varied over a range spanning ±100% of the known values. The first spectral derivative of the experimental absorbance:

$$A_\lambda=-log_{10}[\frac{S_\lambda-DS_\lambda}{R_\lambda-DS_\lambda}] \tag{2.5}$$

was compared with the derivative of theoretical absorbance, calculated as described above and also the second spectral derivative of the absorbance A_λ, was compared with the derivative of the theoretical absorbance using the modified Beer Lambert law (MBLL):

$$A = C \cdot \varepsilon(\lambda) \cdot L \cdot DPF + G \tag{2.6}$$

$$\Delta C = \frac{\Delta A}{\varepsilon(\lambda) \cdot L \cdot DPF} \tag{2.7}$$

where DPF is the differential path length factor [73], L is the physical source detector distance, ΔC is the change in concentration, ΔA is the change in attenuation, and $\varepsilon(\lambda)$ is the specific absorption (extinction) coefficient.

The objective function of the fitting procedure was the norm of residuals for the measured and computed absorbance spectra. The spectral intensity measurements at 2.7 cm source-detector distance were used to obtain the optical properties of the tissue. In this study we used the first and second spectral derivatives of experimental absorbance. The use of the absorbance "A_λ" , which includes the reference signal, eliminated instrumental spectral artifacts and the use of first derivative spectra eliminated unknown factors in source-tissue and detector-tissue couplings, also it helped to magnify the spectral features. The initial values of [HHb] and ($\%FC_{H2O}$) were obtained using the second derivative fit (Figure 2-1), which removed the crosstalk with [$HbO2$]. Then these values were used in the first derivative fit to rectify the values of [HHb] and ($\%FC_{H2O}$) and to obtain the values of [$HbO2$]. This method helped to obtain more accurate values for water concentration and reduced scattering coefficient .

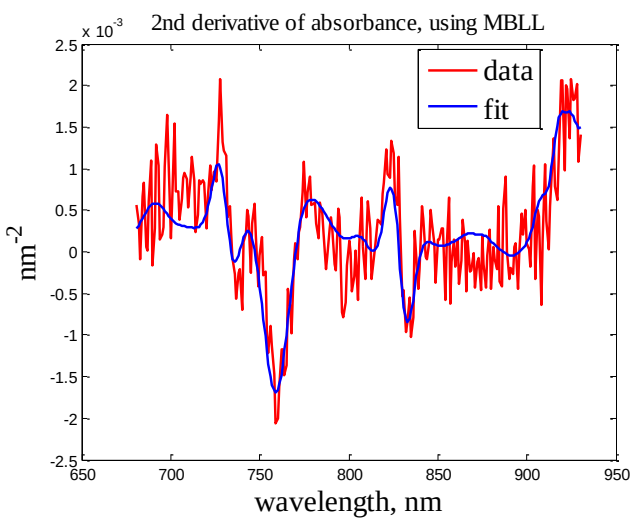

Figure 2-1. Second derivative data fit.

The tissue ICG concentration time course was estimated assuming that other parameters remain constant and CBF was obtained using the following equation:

$$C_{tis}(\mathrm{t}) = \mathrm{CBF} \int_0^t C_a(\tau) R(t-\tau) d\tau \tag{2.8}$$

where, $C_a(t)$ is the arterial ICG concentration measured by a dye densitometer (model DDG-2001 A/K, Nihon Kohden, Tokyo, Japan), $C_{tis}(\mathrm{t})$ is the tissue ICG concentration measured by our optical technique, R(t) is the impulse residue function (IRF) and it has the initial value of one and it decays afterward [74]. By using a de-convolution routine between the two curves of tissue and arterial ICG concentration time course, the IRF curve can be characterized, where the initial height of that, corresponds to the CBF and the area under the curve to the CBV [75]. The de-convolution was applied to each set of $C_a(t)$ and $C_{tis}(\mathrm{t})$ curves individually. The algorithm used physiologically derived constraints to stabilize the retrieved flow-scaled $R(t)$ function [76].

2.3- Results

In order to test our setup we performed experiments with 10% milk as a phantom medium, at two different geometries: an infinite medium (Figure 2-2) and semi-infinite medium (with the boundary condition) (Figure 2-3). Since the NIR absorption of fat was much smaller than the absorption of water, we assumed that the absorption in the phantom medium was only due to the water and the role of the fat was purely scattering. The reduced scattering coefficient μ'_s was measured 3.6 mm^{-1} which was the same value for both geometries, Figure 2-4 (a, b). After dilution of the milk (5 times with water), the μ'_s value reduced to 0.9 mm^{-1} Figure 2-4(c). which was 4 times less than μ'_s for the original 10% milk. This showed a good sensitivity of the system to the scattering properties of the medium.

Figure 2-2. Milk in the film tube Infinite medium (highly scattering), SD = 23 mm

Figure 2-3. Milk in the pan Semi-Infinite medium, SD = 23 mm

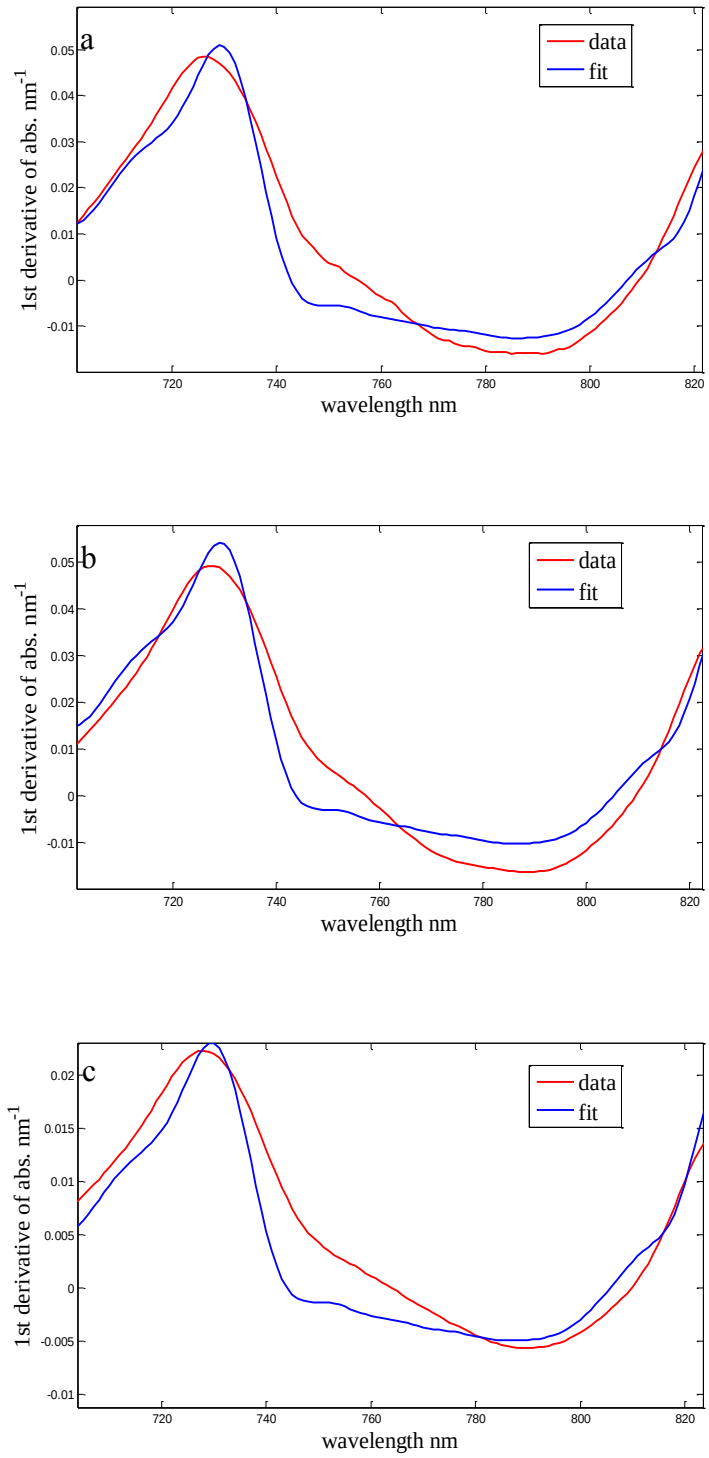

Figure 2-4. First derivative fits for (a) Infinite medium, 10% milk: $\mu'_s = 3.6mm^{-1}$, $(\%FC_{H2O}) = 86\%$ (b) Semi-infinite medium,10% milk: $\mu'_s = 3.6\ mm^{-1}, (\%FC_{H2O}) = 85\%$ (c) Semi-infinite medium, 2% milk: $\mu'_s = 0.9\ mm^{-1}, (\%FC_{H2O}) = 97\%$

In order to obtain the baseline optical properties of head tissue, we measured the reflectance NIR spectra of the piglets' heads and of the pigs open brain after the craniotomy (the probes were placed on the surface of the brain *in vivo*). Figure 2-5, shows a representative example of first derivative spectrum of the attenuation of the pig's open brain and the fit obtained using the diffusion equation for the semi-infinite uniform model. The recovered parameters of the fit are shown in Table 2-1. Note that the average measured cerebral water concentration was 79% $\pm$ 2% which was close to the known value of 80% for juvenile pigs [73].

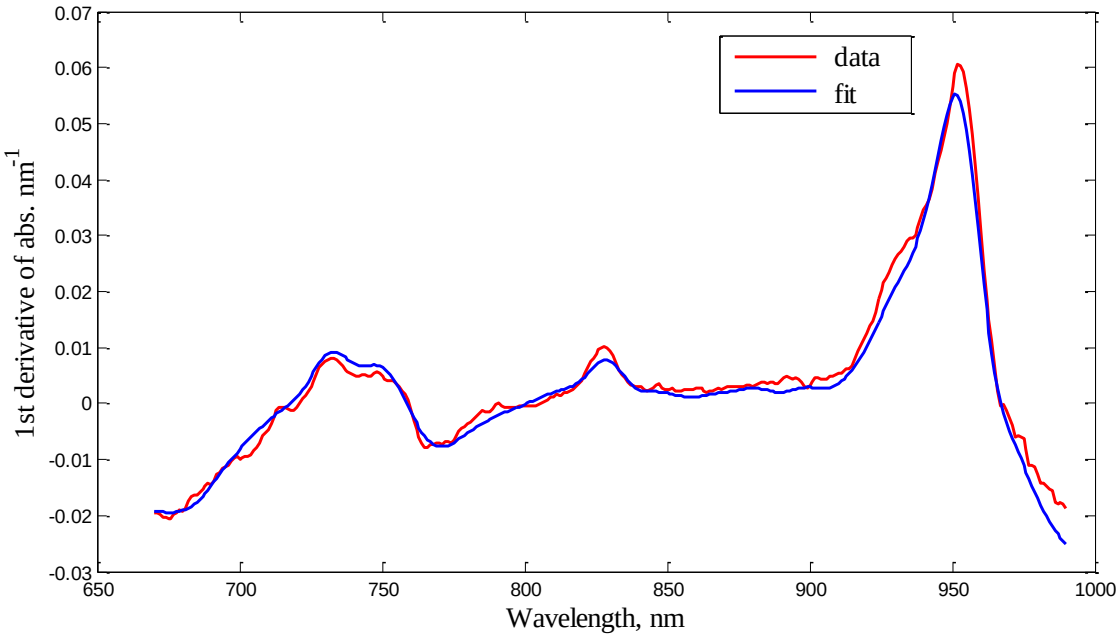

Figure 2-5. First derivative of absorbance for a set of data from pig's open brain fit of the model (blue) to the base line data (red)

Table 2-1. Optical properties of the open brain from recovered parameters of the fit.

Experiment	Oxy Hb μM	Deoxy Hb μM	Water %	μ'_s at 800 nm mm^{-1}	α
1	46	14	80%	0.50	2
2	54	22	81%	0.40	3
3	56	24	77%	0.60	2
4	40	16	78%	0.50	2
5	50	18	79%	0.45	2

Figure 2-6. Shows the first derivative spectrum of the attenuation of the piglet's brain and the fit obtained using the diffusion equation for semi-infinite uniform model at two conditions (baseline and occlusion). The recovered parameters of the fits are shown in Table 2-2.

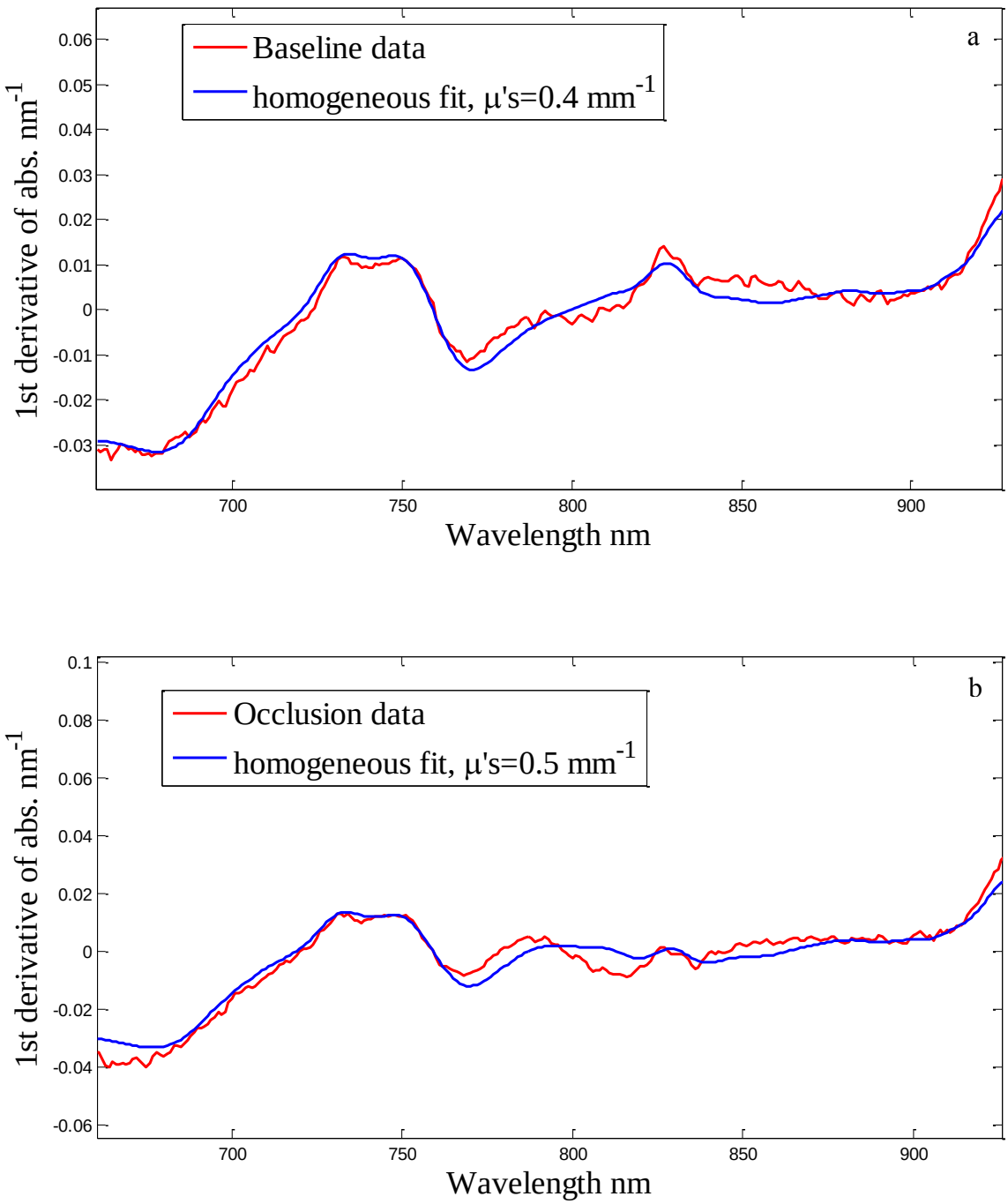

Figure 2-6. Fit of the model (blue) to the baseline data (red) "$R^2 \geq 0.90$" (a): Baseline and (b): Occlusion

Table 2-2. Properties of the piglet brain recovered from the fit, and the cerebral blood flow, blood volume and mean transit time values measured at two different conditions, baseline and occlusion for different animals.

Subject	Oxy (μM)	Deoxy (μM)	Water %	μ'_s at 800nm mm^{-1}	α	CBF (ml/min/100gr)	CBV (ml/100gr)	MTT(s)
Baseline Animal-1	83	18	82	0.45	1.7	69.34	8.69	7.52
Occlusion Animal-1	34	20	85	0.45	1.6	41.34	6.72	9.76
Baseline Animal-2	50	18	86	0.40	1.8	44.75	6.11	8.19
Occlusion Animal-2	15	27	86	0.50	1.6	22.99	6.68	17.44
Baseline Animal-3	50	18	86	0.40	1.8	44.50	5.68	7.66

The obtained water concentration values were in a good agreement with other studies "Woodward & White 1986"[46], "Matcher *et al*, 1994"[24] which gives the average value of 85% for water concentration in the newborn brains.

The obtained values of reduced scattering coefficient μ'_s were also in a reasonable agreement with the values obtained by Fantini *et al.* [77] for human subjects using frequency domain technique.

In order to test our results obtained using the first derivative fit of absorbance by the diffusion equation solution, we also used the second derivative fit of absorbance by the modified Beer

Lambert law. Considering a semi-infinite geometry, the medium DPF was calculated using the following equation: [78].

$$DPF_{si} = \frac{\sqrt{3\mu'_s}}{2\sqrt{\mu_{a0}}} \times \frac{\rho\sqrt{3\mu'_s\mu_{a0}}}{1+\rho\sqrt{3\mu'_s\mu_{a0}}} \tag{2.9}$$

where, ρ is the source detector distance and μ_{a0} is the absorption coefficient at the base line, then we can calculate μ'_s values by using DPF values which we obtained along with deoxy-hemoglobin and water concentration from the second derivative approach. Note that the second derivative approach provides no information about the oxy-hemoglobin concentration value, since the second derivative of the oxy-hemoglobin spectrum does not have any prominent spectral features; hence we used the concentration of oxy-hemoglobin from the first derivative approach to calculate the baseline absorption coefficient μ_{a0}.

Table 2-3. Shows the results of the comparisons between the two approaches. Where subscripts 1 and 2 refer to the 1st and 2nd derivative of absorbance methods.

Table 2-3. The comparison of reduced scattering coefficients obtained from two methods (μ'_{s1} from the fit and μ'_{s2} by calculation from the DPF formula)

	DPF	**HHb, μM**	**Water, %**	μ_{a1}, mm^{-1}	μ_{a2}, mm^{-1}	μ'_{s1}, mm^{-1}	μ'_{s2}, mm^{-1}
Baseline	3.4	21	85	0.021	0.022	0.40	0.46
Occlusion	3.7	20	84	0.013	0.014	0.45	0.42
Baseline	3.6	22	84	0.015	0.016	0.45	0.44

Using measured values of the piglet's brain optical properties, one can recover the ICG time course curves from the signal changes around 810 nm, which corresponds to ICG's absorption peak. Figure 2-7 shows representative examples of ICG time traces. These traces were processed with a de-convolution routine to obtain CBF values shown in the Table 2-2 along with the blood volume and the mean transit time.

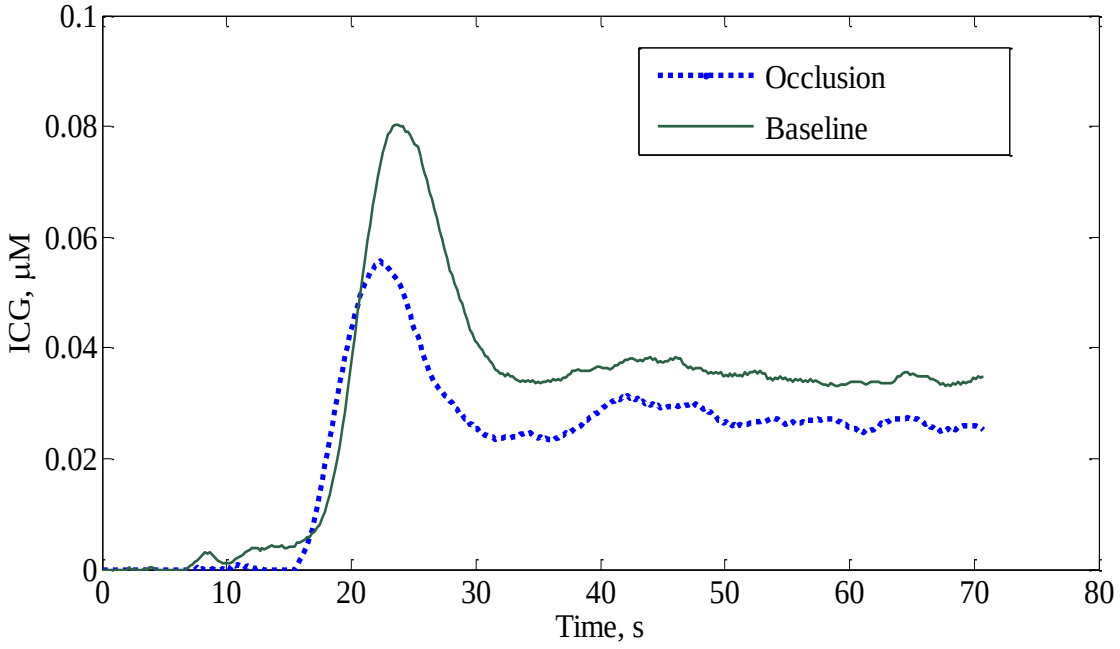

Figure 2-7. Time traces of the brain ICG concentrations during baseline and occlusion

Table 2-4. Shows the comparison of the average cerebral blood flow measured over a range of hemodynamic conditions with the computed tomography (CT) as a gold standard reference (clinically approved and validated technique to measure CBF [79, 80]).

Table 2-4. Comparison of CBF measurement using continuous wave NIRS with CT result

Hemodynamic conditions	Group mean "CBF" NIRS	Group mean "CBF" CT	Mean difference
	$ml/min\ /(100gr)$	$ml/min\ /(100gr)$	$ml/min\ /(100gr)$
Base line	52.9$\pm$4.2	48.3$\pm$1.7	4.6
Occlusion	32.2$\pm$2.9	29.9$\pm$0.9	2.3

2.4- Discussion

Previously we tested our broadband continuous wave approach in a phantom study [63], in which we were able to reconstruct the concentration of the chromophore (carbon black) of homogenous phantoms with the accuracy better than 4% and the values of reduced scattering coefficient with the accuracy 5-10%. In the present study we applied our method *in-vivo*. We have demonstrated the feasibility of a broadband continuous wave spectroscopy technique to obtain baseline optical properties of a homogenous tissue (newborn piglets' brain) *in-vivo* and to reconstruct the ICG concentration changes in the respective tissue with a reasonable accuracy.

The use of spectral derivative was very important for the enhancement of the chromophore spectral features and elimination of the source and detector-surface coupling artefacts, which could cause vertical shifts of the absorbance spectral curves. The advantage of using first derivative of the absorbance was that the concentration of chromophores with less pronounced or broad spectral features, such as oxy-hemoglobin, could be well determined. The required priories for this study were the extinction coefficients spectra of physiologically important chromophores existing in the tissue, as well as ICG's, as an exogenous chromophore. The focus of this work

was to model the wavelength dependent effects of scattering, which enabled us using both first and second spectral derivatives of absorbance data for the analysis. The differential path length factor (DPF) in the brain tissue was obtained 3.57 ± 0.12 from the second spectral derivative technique, which was in good agreement with the previous reports of DPF values in the piglet's brain [81]. In addition we obtained an average cerebral water concentration of $84.3\% \pm 0.5\%$ which was an additional constraint in the first derivative process to obtain more accurate values of reduced scattering coefficient "μ'_s". It is evident that water concentration from both 1st and 2nd derivative techniques were in good agreement with other studies [73]. We used ICG bolus tracking method to measure CBF which was similar in principle to the contrast-enhanced CT and MRI techniques [82].

The value of the reduced scattering coefficient near 800 nm produced the strongest effect on the recovered values of the ICG concentration. On the other hand, the measurement of the scattering properties could not be separated from the measurement of all chromophore concentrations. We obtained the concentrations of oxy-, and deoxy-hemoglobin and water close to those obtained by the frequency-domain technique [61]. In addition, our values of reduced scattering coefficients of the brain tissue (for 27 mm source detector distance) were in the same range obtained by Fantini *et al*. using frequency domain technique (5.2 cm^{-1}) [77]. Moreover, using the baseline parameters, we obtained relatively accurate ICG concentration values, which resulted in reasonable values of CBF.

2.5- Conclusions and Future Works

We obtained reasonable *in-vivo* values of oxy- and deoxy-hemoglobin and water concentrations compared to other studies and techniques. Using our recovered temporal changes of ICG

concentrations with a bolus tracking method, we obtained reasonable CBF, CBV and MTT values according to the respective hemodynamic conditions. Both second derivative, using MBLL, and first derivative, using diffusion equation produced similar baseline values of deoxy-hemoglobin concentrations, which indicated that there was no influence of possible artifacts in our reference signal. Obtaining the values of reduced scattering coefficient and water concentration independently from the first derivative was quite difficult but using the second derivative approach to obtain the water concentration made the values of reduced scattering coefficient more reproducible and reasonable. Our phantom experiment showed a good sensitivity of the system to the scattering properties of the medium.

In future we plan to perform a more detailed analysis of different factors on the accuracy of measured CBF, such as the required accuracy of the extinction spectra of the baseline optical properties and the actual shape of the tissue layers. Moreover, we will apply our broad-band fitting technique, which was earlier successfully tested on the two-layer tissue phantoms, to multilayered geometry of the adult pig head with non-negligible extra cerebral layers and ultimately hope to achieve an adaptation to human studies.

Acknowledgements

This work was supported in part by a grant from the Heart and Stroke Foundation of Canada, a discovery grant from the Natural Science and Engineering Research Council, as well as Ryerson University Research Fund.

Chapter 3

Further Signal Analysis

Improvement of the Algorithm

3.1- Recovering the baseline optical properties using first derivative spectral fit of absorbance

In order to obtain the baseline optical properties using the first spectral derivative fit of the absorbance data by the solution of the diffusion equation, Eq. (2.1), there are five parameters of the fit which are oxy- and deoxy-hemoglobin concentrations ([HbO2], [HHb]), water percentage (wc %), the scattering power (α) and the scattering amplitude at 800 nm which give the reduced scattering coefficient: Eq. (2.4) $\mu'_s(\lambda)=M(\lambda/800)^{-\alpha}$. Due to the cross talk among these parameters at most wavelengths, it is difficult to find the baseline values of parameters accurately from the fit over the entire spectrum of wavelengths. Hence, we studied the influence of each parameter on the first derivative fit by changing the value of that particular parameter while keeping the rest of the parameters fixed (according to the recovered baseline values from the first step).

Figures 3-1 to 3-5, show the plots of differences between the best first derivative fit and the first derivative curves calculated for different values of each parameter while other parameters remained fixed.

The results of the observed changes for the first derivative analysis are shown in Table 3-1.

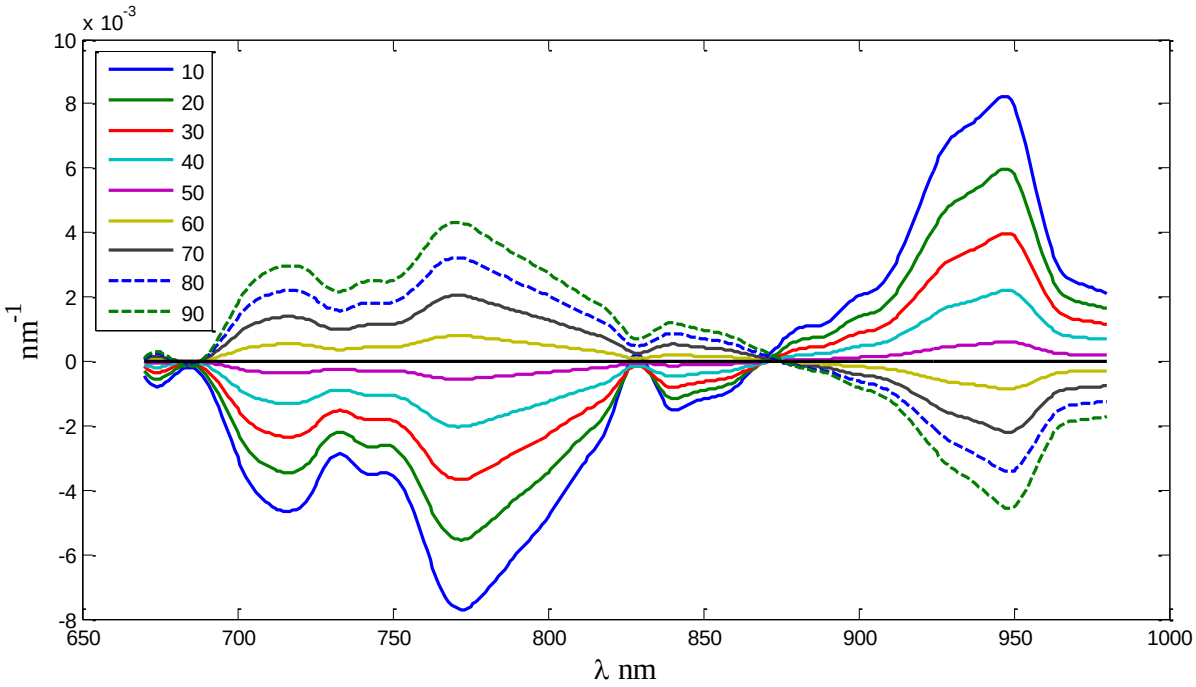

Figure 3-1. Differences between the current first derivative of absorbance and the best baseline curve (52 $\mu\ M$) due to the changes in oxy-hemoglbin from 10 to 90 $\mu\ M$ with intervals of 10$\mu\ M$. Other parameters are kept fixed.

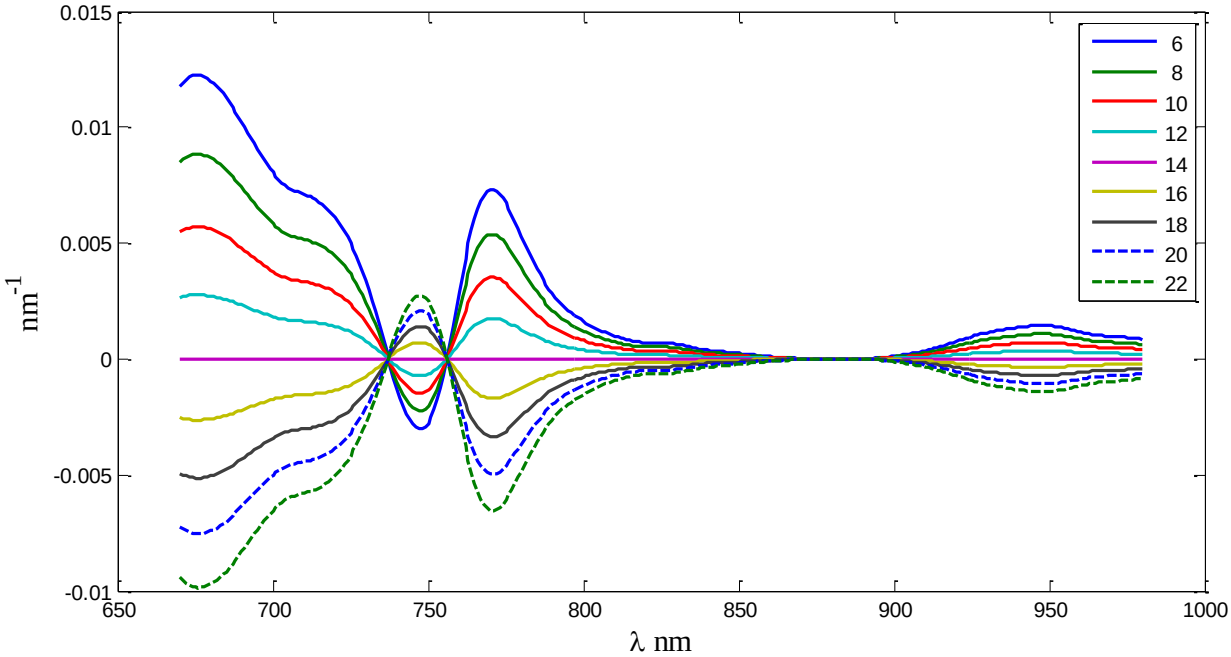

Figure 3-2. Differences between the current first derivative of absorbance and the best baseline curve (14 μM) due to the changes in deoxy-hemoglbin, from 6 to 22 μM with intervals of 2 μM. Other parameters are kept fixed.

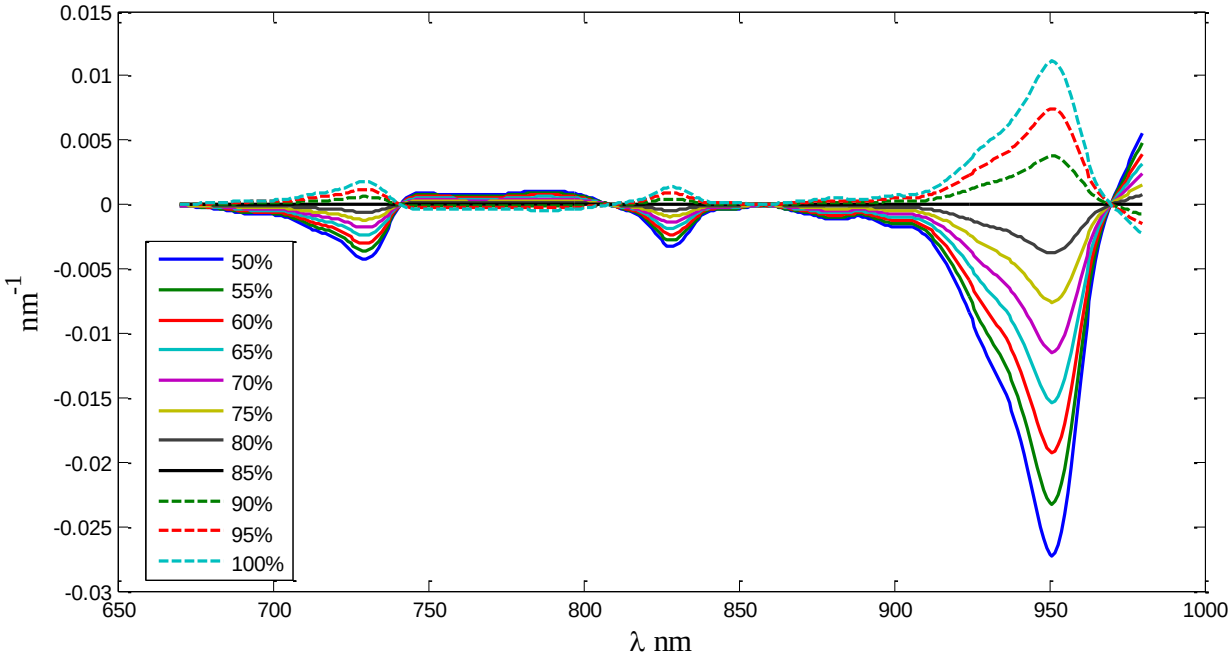

Figure 3-3. Differences between the current first derivative of absorbance and the best baseline curve (85%) due to the changes in water, from 50% to 100% with intervals of 5%. Other parameters are kept fixed.

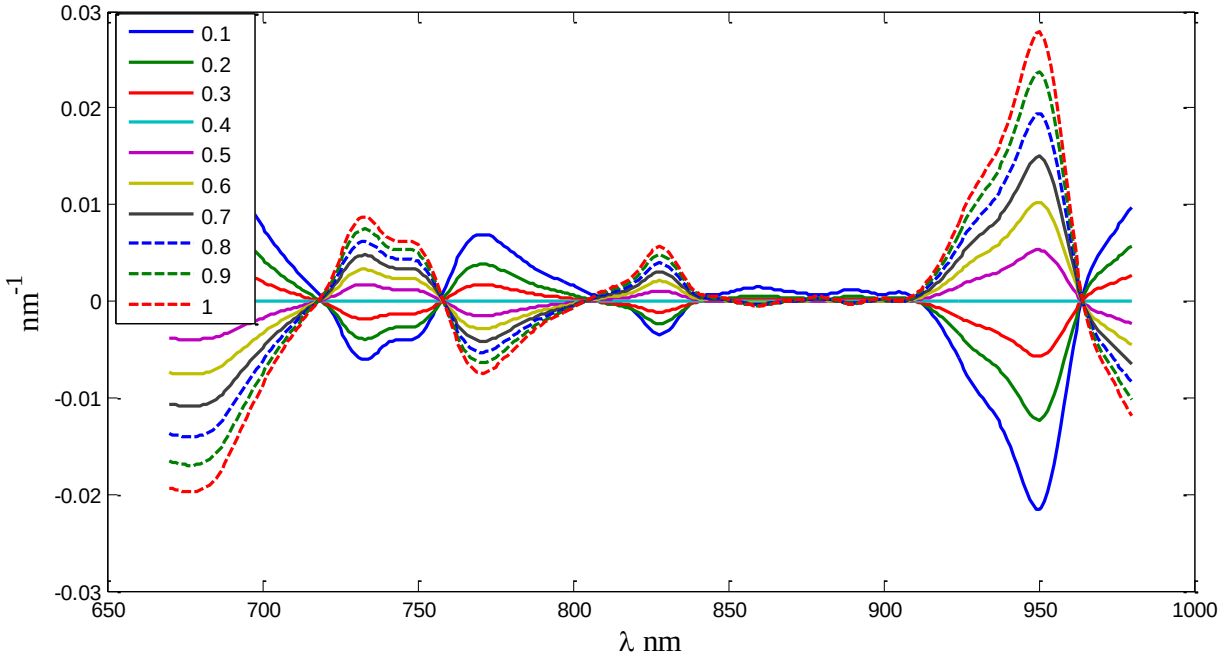

Figure 3-4. Differences between the current first derivative of absorbance and the best baseline curve ($0.4mm^{-1}$) due to the changes in μ'_s , from 0.1 to 1 mm^{-1} with intervals of 0.1 mm^{-1} . Other parameters are kept fixed.

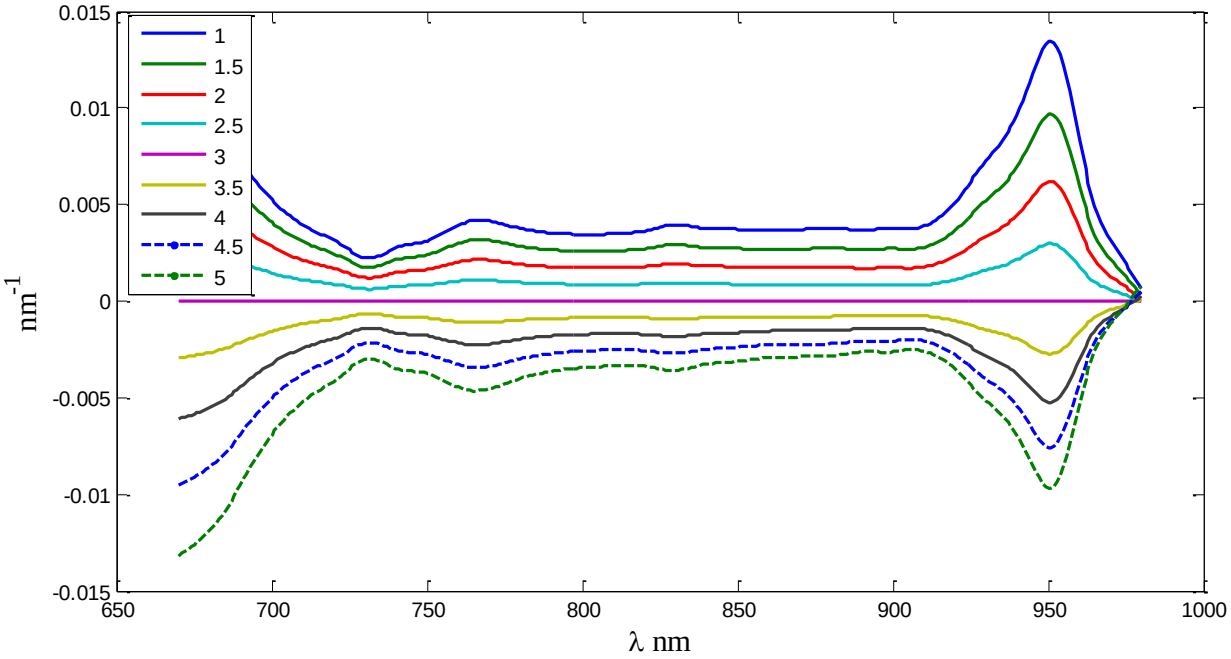

Figure 3-5. Differences between the current first derivative of absorbance and the best baseline curve ($\alpha = 3$) due to the changes in α , from 1 to 5 with intervals of 0.5 . Other parameters are kept fixed.

Table 3-1. Wavelengths at which, the first derivative of absorbance curves, change (anti node), don't change (node or zero), close to the zero (mild node) compared to the baseline.

Wave length nm	water	[HbO2]	[HHb]	M	α
685	Mild-node	Node	Anti-node	Anti-node	Anti-node
742	Node	Anti-node	Anti-node	Anti-node	"
737	Mild -node	Anti-node	Node	Anti-node	"
756	Mild -node	Anti-node	Node	Mild -node	"
808	Node	Anti-node	Anti-node	Node	"
858	Node	Anti-node	Mild node	Mild node	"
871	Mild -node	Node	Node	Mild node	"
842-910	Mild-node	Mild-node	Node (860-900)	Mild node	"

3.2- Recovering the baseline optical properties using second derivative spectral fit of absorbance

The second differential fit analysis of the near infrared reflectance spectrum, using modified Beer-Lambert law with a smaller number of fitting parameters ([HHb], water% and DPF) is faster analysis compared to the first derivative and can be used as an extra constraint in obtaining water content and deoxy-hemoglobin concentration. The same data analysis (change of the differences), were performed for second derivative to find more accurate values for deoxy-hemoglobin and water content.

Figures 3-6 to 3-8 show the plots of the changing behavior of the differences from the baseline values for a representative example set of data while changing one parameter and keeping others fixed at the baseline vales.

The results of the observed changes for the second derivatives are shown in Table 3-2.

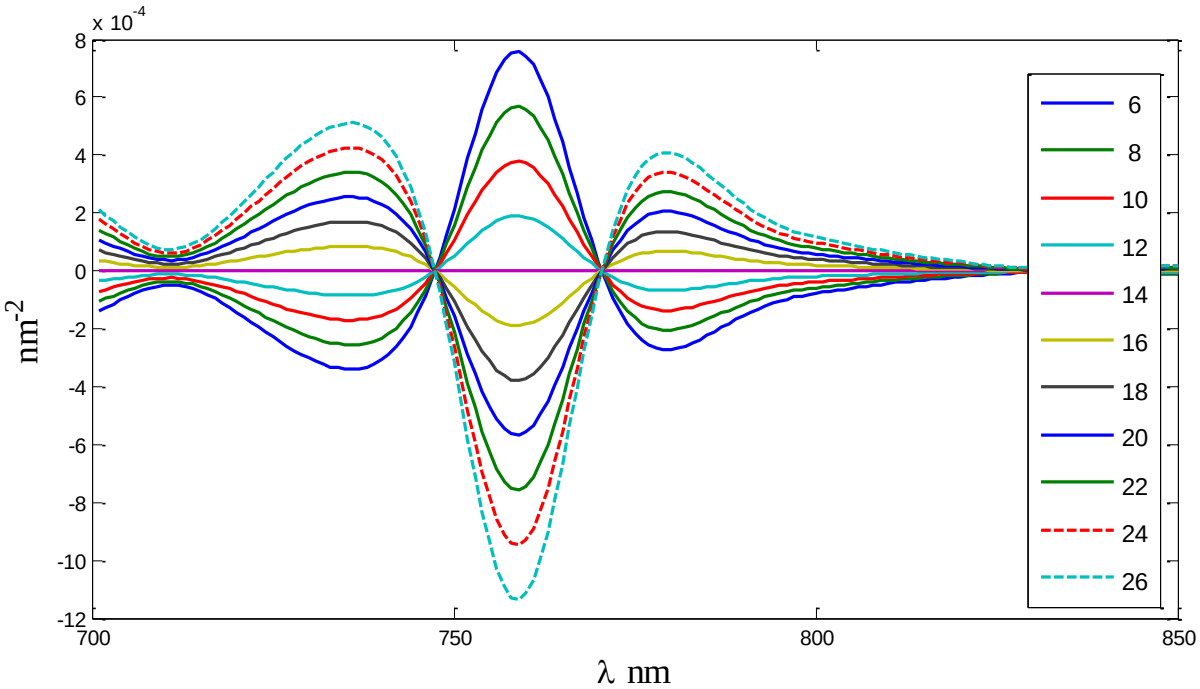

Figure 3-6. Differences between the current second derivative of absorbance and the best baseline curve (14 μM) due to the changes in deoxy-hemoglbin, from 6 to 26 μM with intervals of 2 μM. Other parameters are kept fixed.

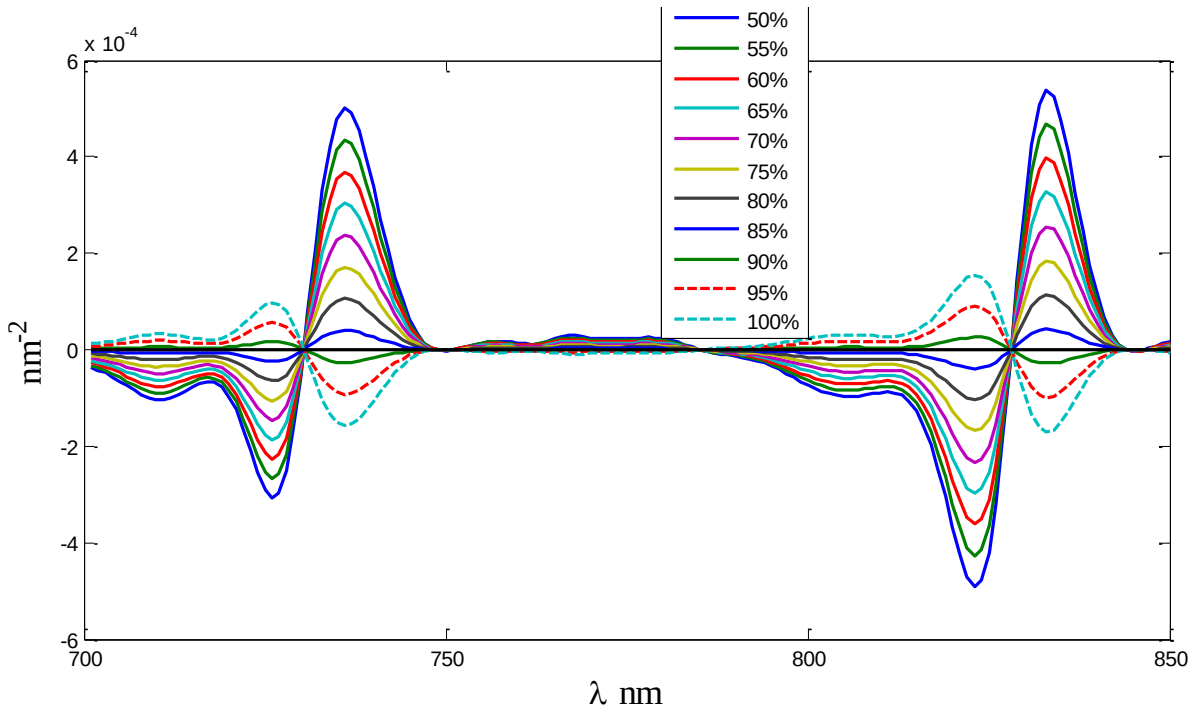

Figure 3-7. Differences between the current second derivative of absorbance and the best baseline curve (87%) due to the changes in water, from 50% to 100% with intervals of 5%. Other parameters are kept fixed.

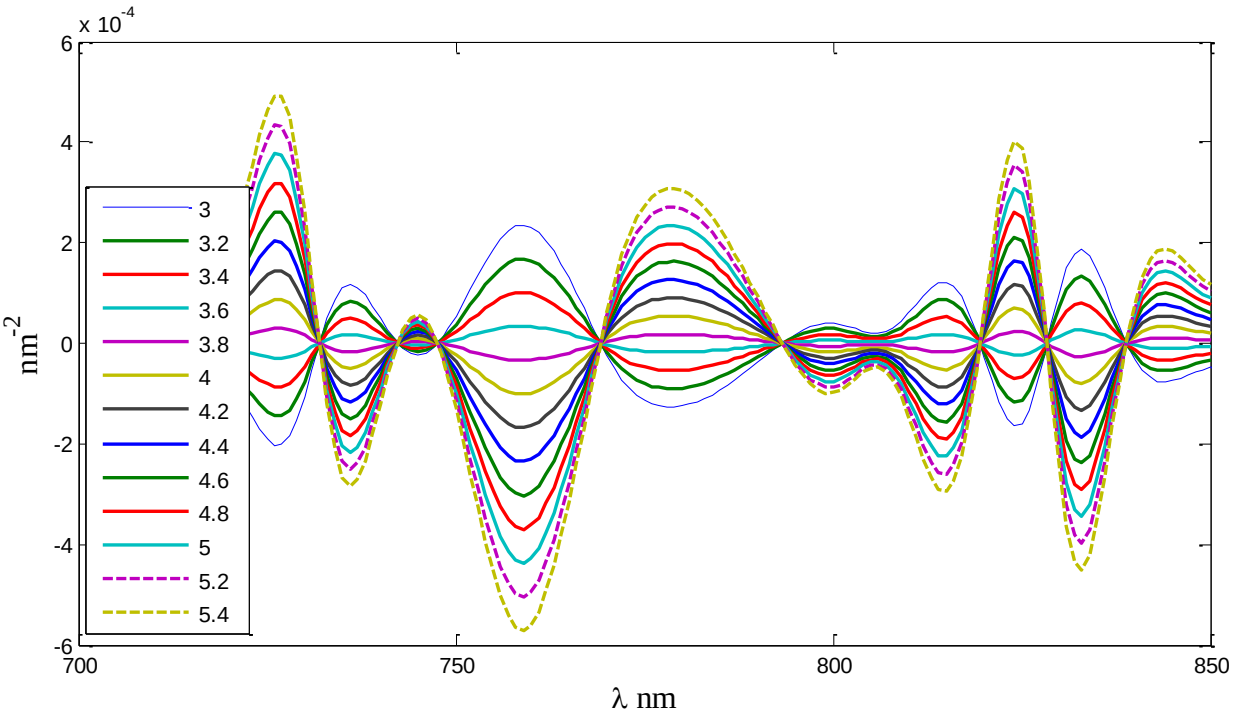

Figure 3-8. Differences between the current second derivative of absorbance and the best baseline curve ($DPF = 3.7$) due to the changes in differential pathlength factor , from 1 to 5.4 with intervals of 0.2 . Other parameters are kept fixed.

Table 3-2. Wavelengths at which, second derivative of absorbance curves, change (anti node), don't change (node or zero), close to the zero (mild node) compared to the baseline.

Wavelength nm	water	[HHb]	DPF
730*	Node	Anti-node	Anti-node
748	Node	Node	Node
770*	Mild-node	Node	Node
825-850	Anti-node	Node	Anti-node
759	Mild node	Anti-node	Anti-node
834	Anti-node	Node	Anti-node
845*	Node	Node	Anti-node
732	Mild-node	Anti-node	Node

Based on Table 3-1, particular wavelengths or wave bands, where some of the parameters are changing and others are fixed, can be considered to modify the value of the changing parameter. For example, after the first step of obtaining the initial baseline values as described in Chapter 2, Section 2.2.3, at wavelength around 808 nm (803-813 nm), one can find a more accurate value for [HbO2] and use that value as a new one to find μ'_s at wavelengths around 871 nm. From the second derivative results (Table 3-2), the values for [HHb] and water can be extracted and used to run in the first derivative package to find final results for the baseline values. Table 3-3 shows the modified results of the analysis for piglets' data.

According to the Table 3-2 information, at 730-732 nm where [HHb] changes but other two parameters (water and DPF) are node or mild node. Hence, we can find a more accurate [HHb] for this region of wavelength from the second derivative analysis fit. Consequently, 770 nm wavelength can be used to fit for water and 845 nm for DPF values. Figure 3-9. Shows flow of the algorithm.

Part 1: Using first derivative of absorbance.

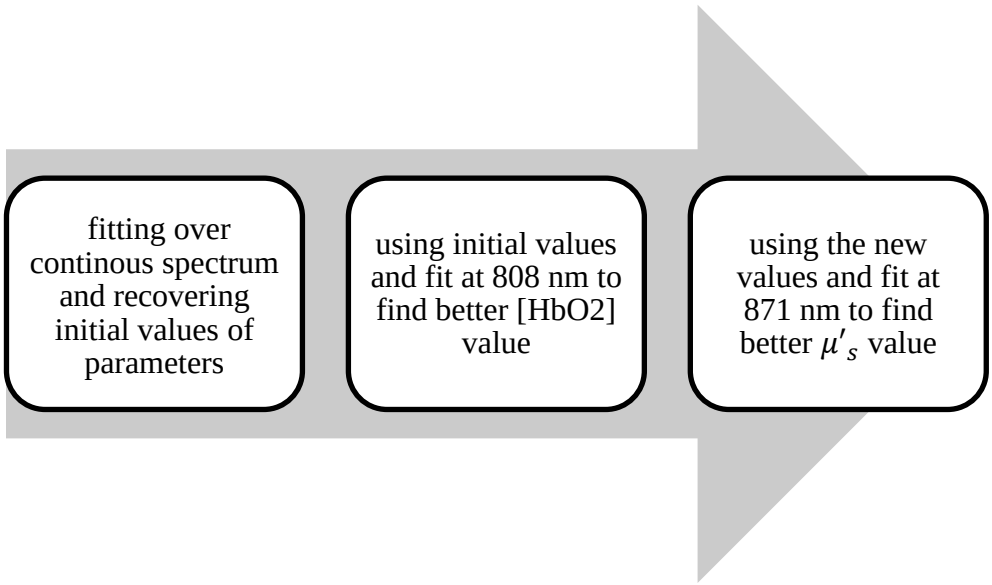

Part 2: Using second derivative of absorbance.

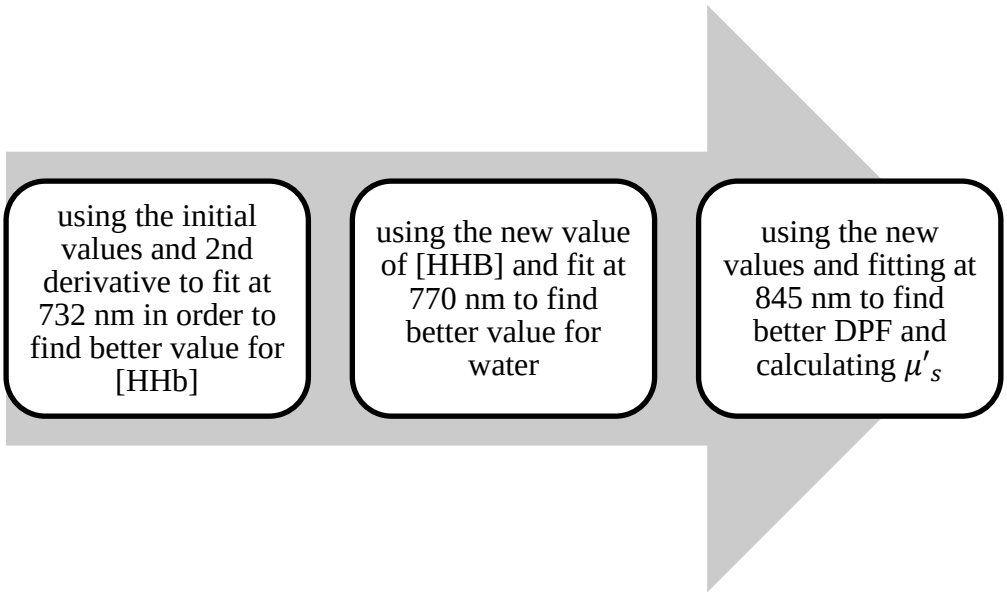

Figure 3-9. Schematic algorithm flow to find baseline values

Table 3-3. The recovered parameters for optical properties of piglets' brain in three different conditions using modified algorithm.

Subject	Oxy (μM)	Deoxy (μM)	Water %	μ'_s (mm^{-1})	α	R^2
Baseline Animal-1	48	18	83	0.50	2.7	0.87
Hypercapnia Animal-1	58	14	82	0.50	2.2	0.91
Occlusion Animal-1	28	16	83	0.60	2.2	0.88
Baseline Animal-2	50	16	84	0.60	2.5	0.92
Hypercapnia Animal-2	54	16	83	0.50	2.5	0.93
Occlusion Animal-2	18	20	84	0.60	2.3	0.89

As we can see the result of reduced scattering coefficients "μ'_s" is very close to the results from Fantini *et al* [77], and the trend of hemoglobin concentration changes is on the right track in accordance with the hemodynamic conditions. Moreover, water concentration has reasonable value and close to the known value of 85% for the newborn brain [24].

"R^2" is the coefficient of determination, and defined as: $R^2 = 1 - \frac{SS_{err}}{SS_{tot}}$, where SS_{err} is the sum of squares of residuals and SS_{tot} is the total sum of squares. The value of R^2 shows the goodness of the fit, which are in the reasonable range of (0.87- 0.93).

Chapter 4

Discussion, Conclusions & Future Works

4.1- Discussion

This study followed previous studies with the same ultimate goal of measuring cerebral hemodynamics, but different techniques and/or approaches.

Our approach was based on broadband continuous wave near infrared spectroscopy technique using analytical solutions of the diffusion equation in order to recover the baseline optical properties of a semi-infinite homogenous tissue (*in vivo* measurement), such as in the newborn piglets' brain. Since the thickness of the tissues overlaying the brain in piglets was about 3 mm or less which was similar to that of newborn infants, these overlying tissues, do not interfere with near infrared monitoring of the brain for the source-detector distance of 27 mm [83]. Hence, the homogeneous assumption was reasonable. Having the baseline optical properties of tissue enabled us to reconstruct the ICG concentration time course changes in the respective tissue.

We used the first and second spectral derivative fits of the absorbance data to eliminate the optical fiber-tissue contact artifacts, to enhance the spectral features of deoxy-hemoglobin and water, which allowed recovering the unknown optical parameters. The use of the first derivative of absorbance has an advantage of recovering the oxy-hemoglobin concentration, which has less pronounced spectral features, as well as recovering the reduced scattering coefficient. The second derivative of absorbance using the modified Beer-Lambert law, although it magnifies the spectral noise, it helps to better recover concentration of deoxy hemoglobin and water as well as the differential path length factor which can be compared with the first derivative results to verify the accuracy of the technique.

In the measurements of the baseline optical properties, a very important factor which could influence the results was the crosstalk in various parameters at most of the wavelengths.

Crosstalk depends on the choice of the wavelengths. A change in [HbO2] may mimic a change in the concentration of deoxy-hemoglobin and vice versa. Hence, crosstalk influences the magnitude and time course of the hemoglobin concentration. In order to overcome this type of crosstalk error, some particular wavelengths were chosen to fit according to the study of each parameter's influence on the spectral derivative curves.

Considering the system set up, geometry, and the protocol of the experiment, there are a number of factors that can degrade the accuracy of the measurement. After preparing the animal, NIRS and CT measurement of CBF were obtained concomitantly to compare over a range of blood flow values by changing the respiratory rate to achieve certain levels of arterial blood CO2 tension (PaCO2), hypocapnia ($\leq 30\, mmHg$), normocapnia ($\approx 40\, mmHg$)and hypercapnia ($\geq 50\, mmHg$). In fact the PaCO2 is the most influential regulator of cerebral circulation [84]. One of the important sources of possible inaccuracy and error which should be taken in to account is the time intervals of the ICG injections. For instance, if this time interval is short, then the ICG still circulates in the system and the accumulation (pile up) effect will happen which may cause uncertainty for the secondary measurements. Also depending on the physiological state of the subject which varies very widely, the response time delay to the changes of hemodynamic conditions could be different and consequently create some loss of precisions in the measurement. Another point is the geometry of the measurement in terms of the source detector distance and position of the probes on the subjects head, whether it is a plane surface or curvature part of the subject's head. Our collaborator team at Lawson Research Institute where the experiments took place, made sure to address all these concerns to minimize the errors associated with the measurements.

Another concern with the near infrared spectroscopy technique is the requirement of ICG injection which is less appealing than using the endogenous chromophores such as oxy and deoxy-hemoglobin. Considering the fact that using oxy-hemoglobin as a tracer involves manipulation of oxygen saturation (SaO2) to produce a bolus of oxy-hemoglobin flowing to the brain which acts as a tracer. This will cause more risk to an already unstable brain injured subject in a clinical settings. Moreover, ICG exhibits much higher signal to noise ratio and more convenient for clinicians to apply. ICG is approved by FDA (Food and Drug Administration) and has many clinical applications to measure various physiological parameters such as cerebral blood flow [85], cardiac output [86], left to right shunts [87], plasma volume [88], and hepatic function [89] and many more in ophthalmology.

In general, our *in vivo* results using the semi-infinite homogenous model by applying a least squares fitting algorithm of the spectral derivative of absorbance data are very encouraging and comparable with other techniques [61, 90].

4.2- Conclusions

Our results using our continuous wave broad band spectral approach to measure absolute optical properties of homogeneous tissue showed good agreement with other near infrared spectroscopy results studies over a range of hemodynamic conditions.

Our new approach is based on the diffusion approximation solution for the semi-infinite homogeneous medium and a least squares fitting algorithm of the first and second spectral derivatives of absorbance data using tabulated chromophore extinction spectra. The optical properties of the newborn piglet's brain and pigs open brain were successfully obtained and the results on CBF measurement using ICG were well correlated with CT results (Table 2-4).

Continuous wave spectroscopic systems offer lower costs and higher signal to noise ratios compared to the time domain and frequency domain systems. Furthermore, a broadband system can resolve more chromophores with more accuracy than a system with limited number of wavelengths. Based on our results we conclude that using a technologically advanced broadband continuous wave NIRS instrument can both yield absolute optical properties of tissue and improve measurements of hemodynamic changes. Our results support the advantage of using near infrared spectroscopy for bedside, safe and non-invasive monitoring of cerebral hemodynamics in neonatal or unstable patients, also the portable nature of the system provides an advantage over conventional CT and MRI scanners for those patients whose condition renders transport unfavorable.

4.3- Future Works

The studies presented above pave the way to new investigations, such as

1) Further validation in older animals with non-negligible extra cerebral layers (ECL). This requires incorporating a multilayered model [91] to account for signal contamination due to ECL as well as partial path length measurement in various layers.

2) One of the important facts which can be of significant concern in the adult head is cerebral spinal fluid (CSF), that always violate the light propagation and approximations (it has a low scattering about 0.1 cm^{-1} and low absorption about 0.021 cm^{-1}, unlike other tissues of ECL). Therefore, more work is required to estimate how uncertainties in scattering and absorption coefficient of CSF (i.e. parametric studies) affect the measurement of CBF and its accuracy.

3) Adaptation of the optical technique to the human studies and more clinical setting.

References

[1] Splinter R., and Hooper B. A. "An Introduction to Biomedical Optics" New York; Taylor & Francis Group (2007).

[2] Wang L. V., and Wu H. "Biomedical Optics: Principle and Imaging," New Jersy: John Wiley & Sons, Inc. (2007).

[3] Aydin E. D., De Oliviera C. R., and Goddard A. J., (2002). A comparison between transport and diffusion calculations using a finite element-spherical harmonics radiation transport method. Medical Physics Vol. 29 no. 9, pp.2013-2023

[4] Pedrotti F. L., and Pedrotti L., Introduction to Optics (3rd Edition). Benjamin Cummings, 3 Ed., (2006).

[5] Taroni P., Pifferi A.,Torricelli A., Comelli D., and Cubeddu R., (2003). In vivo absorption and scattering spectroscopy of biological tissue. Photochemical and Photobiological Sciences: Journal of the European Photochemistry Association and the European Society for Photobiology 2, 124-129

[6] Jacques S. L., Origins of tissue optical properties in the UVA, Visible, and NIR regions, OSA TOPS on Advances in Optical Imaging and Photon Migration , Vol. 2, Alfano R. R., and Fujimoto J. G., Eds., Optical Society of America, Washington, (1996).

[7] Arridge S., " Optical tomography in medical imaging," Inverse Problems, Vol. 15, no. 2, pp. R41-R49, (1999).

[8] Case K. M., and Zweifel P. F., Linear Transport Theory (Addison-Wesley, Reading, Mass.), pp. 196-199

[9] Ishimaru A., Wave Propagation and Scattering in Random Media (Academic New York, 1978), Vol. 1.

[10] Furutsu K., "Diffusion equation derived from space-time transport equation," J. Opt. Soc. Am. 70, 360-366 (1980)

[11] Hiraoka M., Firbank M., Essenpreis M., Cope M., Arridge S., Van Derzee P., and Delpy D., " A Monte Carlo investigation of optical path length in inhomogeneous tissue and its application to near infrared spectroscopy," Physics in Medicine and Biology, Vol. 38, no. 12, pp. 1859-1876, (1993).

[12] Delpy D. T., Cope M., Van Der Zee P., Arridge S., Wray S., and Wyatt J., "Estimation of optical path length through tissue from direct time of flight measurement.," Physics in Medicine and Biology, Vol.33, no.12, pp. 1433-1442, (1988).

[13] Groenhuis R., Ferwerda H., and Ten Bosch J., "Scattering and absorption of turbid materials determined from reflection measurements." Applied Optics, Vol. 22 no. 16, pp. 2456-2462, (1983).

[14] Alexandrakis G., Farrel T. J., Patterson M. S. (2000). Monte Carlo diffusion hybrid model for photon migration in a two- layer turbid medium in the frequency domain, Applied Optics 39, 2235-2244

[15] Gratton E., Fantini S., Franceschini M. A., Gratton G., and Fabiani M., (1997). Measurements of scattering and absorption changes in muscle and brain. Philosophical Transactions of the Royal Society of London.Series B, Biological Sciences 352, 727-735

[16] Son I. Y., and Yazici B., " Near infrared imaging and spectroscopy for brain activity monitoring," NATO Security through Science Series A: Chemistry and Biology, pp. 341-372, (2006)

[17] Jobsis F. F., (1977) Non-invasive infrared monitoring of cerebral and myocardial oxygen sufficiency and circulatory parameters. Science 198:1264-1267

[18] Brazy J. E., Lewis D. V., (1986) Changes in cerebral blood volume and cytochrome aa3 during hypertensive peaks in preterm infants. Pediatrics 108:983-987

[19] Ferrari M., De Marchis C., Giannini I., DiNicola A., Agostino R., Nodari S., Bucci G. (1986) cerebral blood volume and hemoglobin oxygen saturation monitoring in neonatal brain by near infrared spectroscopy. Adv Exp Med Biol 200:203-211

[20] Cope M., Delpy D. T., (1988) System for long-term measurement of cerebral blood and tissue oxygenation on newborn infants by near infrared transillumination. Med Biol Eng Comput 26:289-294

[21] Gratton E., Toronov V., Wolf M., Wolf U., Webb A., (2005).Measurement of brain activity by near infrared light. Journal of Biomedical Optics, 10, 1, 011008-13.

[22] Jasdzewski G., Strangman G., Wagner J., Kwong K.K., Poldrack R.A., Boas D.A., (2003). Differences in the hemodynamic response to event-related motor and visual paradigms as measured by near infrared spectroscopy. NeuroImage, 20, 479-488.

[23] Arridge S.R., Optical tomography in medical imaging , Inverse Problems 15, R1-R53 (1999).

[24] Matcher S. J., Cope M., Delpy D. T., "Use of the water absorption spectrum to quantify tissue chromophore concentration changes in near infrared". Phys Med Biol. (1994) Jan;39(1):177-196.

[25] J. Selb, A.M. Dale, and D.A. Boas, "Linear 3D reconstruction of time-domain diffuse optical imaging differential data: improved depth localization and lateral resolution,"Opt. Express 15, 16400-16412 (2007).

[26] S. Fantini, M. A. Franceschini, J. S. Maier, S. A. Walker, B. Barbieri, and E. Gratton, "Frequency Domain Multichannel Optical Detector for Non-Invasive Tissue Spectroscopy and Oximetry," Opt. Eng. 34, 32-42 (1995)

[27] Pucci O., Toronov V., St. Lawrence K., "Measurement of the optical properties of a two-layer model of the human head using broadband near-infrared spectroscopy", J. of Biomed. Optics (2009)

[28] Bevilacqua F., Berger A. J., Cerussi A. E., Jakubowski D., Tromberg B. J., "Broadband absorption spectroscopy in turbid media by combined frequency-domain and steady-state methods," Appl Opt. (2000) Dec1; 39(34):6498-6507

[29] Bozkurt A., Rosen A., Rosen H., and Onaral B., (2005). “A portable near infrared spectroscopy system for bedside monitoring of newborn brain,” Biomedical Engineering. Vol. 4, no. 29.

[30] Bunce S. C., Izzetoglu M., Izzatuglo K., Onaral B., and Pourrezaei K., (2006). “Functional near infrared spectroscopy,” IEEE Engineering in Medicine and Biology Magazine; The Quarterly Magazine of the Engineering in Medicine and Biology Society 25, pp. 54-62

[31] Jacob M., Bresler Y., Toronov V., Zhang X., and Webb A., (2006). Level-set algorithm for the reconstruction of functional activation in near infrared spectroscopic imaging. Journal of Biomedical Optics 11, 064029

[32] Chance B., Anday E., Nioka S., Zhou S., Hong L., Worden K., Li C., Murray T., Ovetsky Y., Pidiklti D., and Thomas R., “A novel method for fast imaging of brain function, non-invasively, with light,” Optics Express, V0l. 2, no 10, pp. 411-423, (1998)

[33] Boas D. A., Brooks D H., Miller E. H., DiMarzio C A., Kilmer M., and Gaudette R. J., “Imaging the body with diffuse optical tomography.” Signal Processing Magazine, IEEE. Vol. 18, no.6 pp. 57-75, (2001).

[34] Chance B., Nioka S., Kent J., McCully K., Fountain M., Greenfeld R., and Holtom G., “Time resolved spectroscopy of hemoglobin and myoglobin in resting and ischemic muscle,” Analytical Biochemistry, Vol. 174, no. 2 pp. 698-707, (1988)

[35] Delpy D. T., and Cope M., “Quantification in tissue near infrared spectroscopy,” Philosophical Transaction of the Royal Society of London Series B-Biological Sciences 352, 649-659 (1997).

[36] Rolfe P., (2000). “In vivo near infrared spectroscopy,” Annual Review of Biomedical Engineering 2, pp. 715-754

[37] Hoshi Y., “Functional near infrared optical imaging: Utility and limitation in human brain mapping,” Psychophysiology, Vol. 40 no. 4 pp. 511-520 (2003).

[38] Groenhuis R.A., Ferwerda H.A., and Ten Bosch J.J., (1983). “Scattering and absorption of turbid materials determined from reflection measurements.”Applied Optics 22, 2456

[39] Kim J.G., Xia M., and Liu H., (2005). "Extinction coefficients of hemoglobin for near infrared spectroscopy of tissue," IEEE Engineering in Medicine and Biology Magazine: The Quarterly Magazine of the Engineering in Medicine & Biology Society 24, pp. 118-121.

[40] Workman J., and Weyer L., Practical Guide to Interpretive Near Infrared Spectroscopy. Taylor and Francis Group (2008)

[41] Sassaroli A., and Fantini S., "Comment on the modified Beer-Lambert law for scattering media," Physics in Medicine and Biology, Vol. 49, no. 14 pp. 255-257, (2004)

[42] Raynolds E. O. R., Wyatt J. S., Azzopardi D., Delpy D. T.,Cady E. B., Cope m., and Wray S., " New non-invasive methods for assessing brain oxygenation and hemodynamics," British Medical Bulletin, Vol. 44, (1988)

[43] Obrig H., and Villringer A., "Beyond the visible - imaging the human brain with light," Journal of Cerebral Blood Flow and Metabolism, Vol. 23, no.1 pp. 1-18 (2003)

[44] Bolin F. P., Preuss L. E., Taylor, R. C., and Ference R. (1989): Appl. Opt. 28, pp. 2297-2302

[45] Arridge S. R., Cope, M., and Delpy D. T., (1992): Phys. Med. Bio. Vol. 37, pp. 1531-1560

[46] Woodward H. Q., and White D. R., (1986) "The composition of body tissues" Br. J. Radiol. Vol. 59 pp. 1209-1219

[47] Essenpreis M., Elwell C. E., Cope M., Van der Zee P., Arridge S. R., and Delpy D. T., (1993): Appl. Opt. 32, pp. 418-425

[48] Van der Zee P., Arridge S. R., Cope M., and Delpy D. T., (1990): Adv. Exp. Med. & Biol. 277, pp. 79-84

[49] Germon T. J., Young A. E., Nelson R. J., (1995). Near infrared spectroscopy. Journal of Neurosurgery 83(6), pp. 1111-12

[50] Edvinsson L., and Krause D.N., eds., "Cerebral Blood Flow and Metabolism," (Lippincott Williams and Wilkins, Philadelphia 2001).

[51] Villringer A., and Chance B., (1997). “Non invasive optical spectroscopy and imaging of human brain function,” Trends in Neurosciences 20, pp. 435-442

[52] Izzetoglu M., Bunce S. C., Izzatuglo K., Onaral B., and Pourrezaei K., (2007). “Functional brain imaging using near infrared technology,” IEEE Engineering in Medicine and Biology Magazine; The Quarterly Magazine of the Engineering in Medicine and Biology Society 26, pp. 38-46

[53] Young A. E., Germon T. J., Barnet N. J., Manara A. R., and Nelson R. J., (2000). “Behavior of near infrared light in the adult human head: implications for clinical near infrared spectroscopy,” British Journal of Anaesthesia 84, pp. 38-42

[54] Wolf M., *et al* (2008). “Near infrared spectroscopy to study the brain”: an overview. Opto-Electroncs Review 16, pp. 413-419.

[55] Stepnoski R. A., LaPorta A., Raccuia-Behling F., Blonder G. E., Slusher R. E., and Kleinfeld D., (1991) “Non-invasive detection of changes in membrane potential in cultured neurons by light scattering,” Proceedings of the National Academy of Sciences of the United States of America 88, pp. 9382-9386

[56] Marin T, Moore J., “Understanding near-infrared spectroscopy”. Adv. Neonatal Care. (2011) Dec;11(6):382-8.

[57] Patel J., Marks K., Roberts I., Azzopardi D., and Edwards A.D., “Measurement of cerebral blood flow in newborn infants using near infrared spectroscopy with Indocyanine Green,” Pediatr. Res. 43, pp.34-39 (1998).

[58] Gora F., Shinde S., Elwell C.E., Goldstone J.C., Cope M., Delpy D.T., and Smith M.,” Non-invasive measurement of cerebral blood flow in adults using near infrared spectroscopy and Indocyanine Green: a pilot study,” J. Neurosurg. Anesthesiol. 14, pp. 218-222 (2002).

[59] Haruna M., Kumon K., Yahagi N., Watanabe Y., Ishida Y., Kobayashi N., and Aoyagi T., “Blood volume measurement at the bedside using ICG pulse spectrophotometry,” Anesthesiology 89, pp. 1322-1328 (1998).

[60] Landsman M. L. J., Kwant G., Mook G. A., Zijlstra W. G., "Light- absorbing properties, stability, and spectral stabilization of indocyanine green," J. Appl. Physiol.,40, 575-583 (1976).

[61] Choi, J., M. Wolf, V. Toronov, U. Wolf, C. Polzonetti, D. Hueber, (2004). “Noninvasive determination of the optical properties of adult brain: near-infrared spectroscopy approach,” Journal of Biomedical Optics 9, 221-229.

[62] Hunter, R.J., M.S. Patterson, T.J. Farrell & J.E. Hayward. (2002). “Haemoglobin oxygenation of a two-layer tissue-simulating phantom from time-resolved reflectance: effect of top layer thickness,” Physics in Medicine and Biology 47, 193-208.

[63] Pucci O., *et al*, “Measurement of the optical properties of a two-layer model of the human head using broadband near-infrared spectroscopy”, Applied Optics, 49, 6324-6332 (2010).

[64] Nabavi D.G. *et al*, “Window narrowing: a new method for standardized assessment of the tissue at risk-maximum of infarction in CT based brain perfusion maps”, Neurol Res. 29, 296-303 (2007).

[65] Diop M., *et al*, “A broadband continuous-wave multichannel near-infrared system for measuring regional cerebral blood flow and oxygen consumption in newborn piglets,” Rev. Sci. Instrum. 80, 054302 (2009).

[66] S. Chandrasekhar, Radiative Transfer (Oxford U. Press, New York, 1960).

[67] V. V. Sobolev, A. Treatise, on Radiative Transfer (Van Nostrand-Reinhold, Prinston, N. J., 1963)

[68] K. M. Case, and P. Z. Zweifel, Linear Transport Theory (Addison-Wesley, Reading, Mass., 1967) pp. 196-199.

[69] A. Ishimaru, “Wave Propagation and Scattering in Random Media,”(Academic, New York, 1978), Vol. 1

[70] S. Fantini, M. A. Franceschini and E. Gratton " Semi-infinite geometry boundary problem for light migration in highly scasttering media:a frequency domain study in the diffusion approximation" J. Opt. Soc. Am. B/Vol. 11.No 10/ (1994)

[71] Patterson M. S., *et al*, "Time resolved reflectance and transmittance for the non-invasive measurement of tissue optical properties", Applied Optics 28,12 (1989).

[72] Kienle A., Patterson M. S., "Improved solutions for the steady state and the time resolved diffusion equations for reflectance from a semi- infinite turbid medium", J. Opt. Soc. Am. Vol. 14 (1997)

[73] Delpy D.T., Cope M., Van der Zee P., Arridge S.,Wray S., Wyatt J.S., 1988 "Estimation of optical pathlength through tissue from direct time of flight measurement," Phys Med Biol 33:1433-1442

[74] Elliott J.T., *et al*, "Quantitative measurement of cerebral blood flow in a juvenile porcine model by depth-resolved near-infrared spectroscopy", J. Biomed Opt. 15, 037014 (2010).

[75] Brown D. W., *et al*, "Quantitative near infrared spectroscopy measurement of cerebral hemodynamics in newborn piglets", Pediatric Research Vol. 51 (2002)

[76] J. T. Elliott, M. Diop, T. Y. Lee, and K. S. Lawrence, "Model-independent dynamic constraint to improve the optical reconstruction of regional kinetic parameters," Opt. Lett. 37, 2571-2573.

[77] Fantini S., *et al*, "Absolute optical measurements of cerebral optical coefficients and hemoglobin concentrations in aging and younger human subjects" Biomedical Optics (BIOMED) (2012) paper: BTu3A.61

[78] Fantini S., *et al*, "Non-invasive optical monitoring of the newborn piglet brain using continuous wave and frequency domain spectroscopy" Phys Med Biol. (1999) Jun;44(6):1543-63.

[79] A. A. Konstas, G. V. Goldmakher, T. Y. Lee, and M. H. Lev, "Theoretic basis and technical implementations of CT perfusion in acute ischemic stroke. Part 1: technical implementations," AJNR Am. J. Neuroradiol. 30(4). 662-668 (2009)

[80] A. A. Konstas, G. V. Goldmakher, T. Y. Lee, and M. H. Lev, “Theoretic basis and technical implementations of CT perfusion in acute ischemic stroke. Part 2: technical implementations,” AJNR Am. J. Neuroradiol. 30(5). 885-892 (2009)

[81] R. Springett, Y. Sakata, and D. T. Delpy, “Precise measurement of cerebral blood flow in newborn piglets from the bolus passage of indocyanine green,” Phys Med Biol 46(8) 2209-2225 (2001)

[82] M. Wintermark, M. Sesay, E Barbier, K Borbely, W. P. Dillon, J.D. Eastwood, T.C. Glenn, C.B. Grandin, S. Pedraza, J. F. Soustiel, T. Nariai, G. Zaharchuk, J. M. Caille, V. Dousset, and H. Yonas, “Comparative overview of brain perfusion imaging techniques,” Stroke 36(9),e83-99 (2005)

[83] D.A. Benaron, C.D. Kurth, J.M. Steven, M. Delivoria-Papadopoulos, B. Chance (1995) ”Transcranial optical path length in infants by near infrared phase-shift spectroscopy” J. Clin. Monit. Comput. Vol.11. pp.109-117

[84] van Bel F., van de Bor M., Baan J., Ruys J.H. (1998) “The influence of abnormal blood gases on cerebral blood flow velocity in the preterm newborn”. Neuropediatrics Vol. 19 pp.27-32

[85] J. Patel, K. Marks, I. Roberts, D. Azzopardi, A.D. Edwards, (1998) “Measurement of cerebral blood flow in newborn infants using near infrared spectroscopy with Indocyanine Green,” Pediatr Res. Vol. 43 pp. 34-39

[86] A. J. O’Connell, J. Tibballs, M. Coulthard, (1991): “Improving agreement between thoracic bioimpedance and dye dilution cardiac output estimation in children,” Anaesth. Intensive Care Vol. 19 pp. 434-440

[87] L. J. Krovetz, I. H. Gessner, (1965) “A new method utilizing indicator dilution techniques for estimation of left to right shunts in infants”. Circulation Vol. 32 pp. 772-777

[88] M.Y. Anthony, S.R. Goodall, M. Papouli, M.I. Levene, (1992) “Measurement of plasma volume in neonates”. Arch. Dis. Child Vol. 67 pp. 36-40

[89] W. E. Evans, M. V. Relling, S. de Graff, J. H. Rodman, J. A. Pieper, M. L. Christensen, W.R. Crom, (1989) “Hepatic drug clearance in children: studies with indocyanine green as a model substrate”. J. Pharm. Sci. Vol. 78 pp. 452-456

[90] M. Diop, K. M. Tichauer, J. T. Elliot, “Comparison of time-resolved and continuous wave near infrared techniques for measuring cerebral blood flow in piglets” J.B.O. (2010) Vol. 15(5)

[91] A. Kienle, M. S. Patterson, N. Dognitz, R. Bays, G. Wagnieres, and H. van den Bergh, “Non-invasive determination of the optical properties of two-layered turbid media,” Appl. Opt. Vol. 37(4). pp. 779-791 (1998).